Ion acceleration and coherent structure formation following laser pulse self-channeling

Andrea Macchi

www.df.unipi.it/∼macchi

polyLAB, CNR-INFM, University of Pisa, Italy

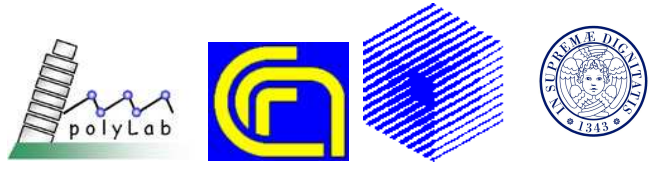

EPS Conference on Plasma Physics, Warsaw, July 2, 2007

Coworkers

Coworkers

Alessandra Bigongiari, Francesco Ceccherini, Fulvio Cornolti,Tatiana V. Liseykina[1]

Department of Physics, University of Pisa, Italy

Coworkers

Alessandra Bigongiari, Francesco Ceccherini, Fulvio Cornolti,Tatiana V. Liseykina[1]

Department of Physics, University of Pisa, Italy

[1] *On leave from Institute for Computational Technologies, Novosibirsk, Russia*

Coworkers

Alessandra Bigongiari, Francesco Ceccherini, Fulvio Cornolti,Tatiana V. Liseykina[1]

Department of Physics, University of Pisa, Italy

[1] *On leave from Institute for Computational Technologies, Novosibirsk, Russia*

Marco Borghesi, Satyabrata Kar, Lorenzo Romagnani

IRCEP and School of Mathematics and Physics, Queen's University of Belfast, UK

Outlook

Outlook

- Motivations and simulation set-up

Outlook

- Motivations and simulation set-up
- Ion dynamics after self-channeling

Outlook

- Motivations and simulation set-up
- Ion dynamics after self-channeling
  - “breaking” of channel walls

Outlook

- Motivations and simulation set-up
- Ion dynamics after self-channeling
  - “breaking” of channel walls
  - electric “echo” effect

Outlook

- Motivations and simulation set-up
- Ion dynamics after self-channeling
  - “breaking” of channel walls
  - electric “echo” effect
  - laser beam breakup

Outlook

- Motivations and simulation set-up
- Ion dynamics after self-channeling
  - “breaking” of channel walls
  - electric “echo” effect
  - laser beam breakup
- Coherent structure generation

Outlook

- Motivations and simulation set-up
- Ion dynamics after self-channeling
  - “breaking” of channel walls
  - electric “echo” effect
  - laser beam breakup
- Coherent structure generation
  - structure patterns in plasma channels

Outlook

- Motivations and simulation set-up
- Ion dynamics after self-channeling
  - “breaking” of channel walls
  - electric “echo” effect
  - laser beam breakup
- Coherent structure generation
  - structure patterns in plasma channels
  - “hybrid” vortex-soliton structures

Motivations

Motivations

- Proton diagnostic techniques allow to detect electric and magnetic fields in laser plasmas with picosecond resolution

Motivations

- Proton diagnostic techniques allow to detect electric and magnetic fields in laser plasmas with picosecond resolution
- Investigation of nonlinear laser-plasma dynamics, particularly coherent structures (solitons, vortices) generation is now possible

Motivations

- Proton diagnostic techniques allow to detect electric and magnetic fields in laser plasmas with picosecond resolution
- Investigation of nonlinear laser-plasma dynamics, particularly coherent structures (solitons, vortices) generation is now possible
- Simulations of laser-plasma interaction need to reach picosecond time scales (thousands of laser periods)

Motivations

- Proton diagnostic techniques allow to detect electric and magnetic fields in laser plasmas with picosecond resolution
- Investigation of nonlinear laser-plasma dynamics, particularly coherent structures (solitons, vortices) generation is now possible
- Simulations of laser-plasma interaction need to reach picosecond time scales (thousands of laser periods)
- Need to address the effect of ion motion on field structures for such time scales

Simulation set-up

Simulation set-up

Particle-in-Cell (PIC) simulations in 2D cartesian geometry

Simulation set-up

Particle-in-Cell (PIC) simulations in 2D cartesian geometry

Laser amplitude $a_L = 1.7 \div 2.7$
duration $\tau_L = 150 \div 300 T_L$ $\qquad (T_L = \lambda/c)$
$\Rightarrow \;\; I = 10^{18} \div 10^{19}$ W/cm^2,
$\tau_L = 0.5 \div 1$ ps for $\lambda = 1\ \mu$m.
S-polarization (E_z)

Simulation set-up

Particle-in-Cell (PIC) simulations in 2D cartesian geometry

Laser amplitude $a_L = 1.7 \div 2.7$
duration $\tau_L = 150 \div 300 T_L$ $\qquad (T_L = \lambda/c)$
$\Rightarrow \;\; I = 10^{18} \div 10^{19}$ W/cm^2,
$\tau_L = 0.5 \div 1$ ps for $\lambda = 1\ \mu$m.
S-polarization (E_z)

Inhomogenous plasma
Peak density $n_e = 0.1 n_c$
Size $S = 500\ \lambda$
Scalelenght $L = 400\ \lambda$

Simulation set-up

Particle-in-Cell (PIC) simulations in 2D cartesian geometry

Laser amplitude $a_L = 1.7 \div 2.7$
duration $\tau_L = 150 \div 300 T_L$ $\quad (T_L = \lambda/c)$
$\Rightarrow \; I = 10^{18} \div 10^{19}$ W/cm^2,
$\tau_L = 0.5 \div 1$ ps for $\lambda = 1$ μm.
S-polarization (E_z)

Inhomogenous plasma
Peak density $n_e = 0.1 n_c$
Size $S = 500\ \lambda$
Scalelenght $L = 400\ \lambda$

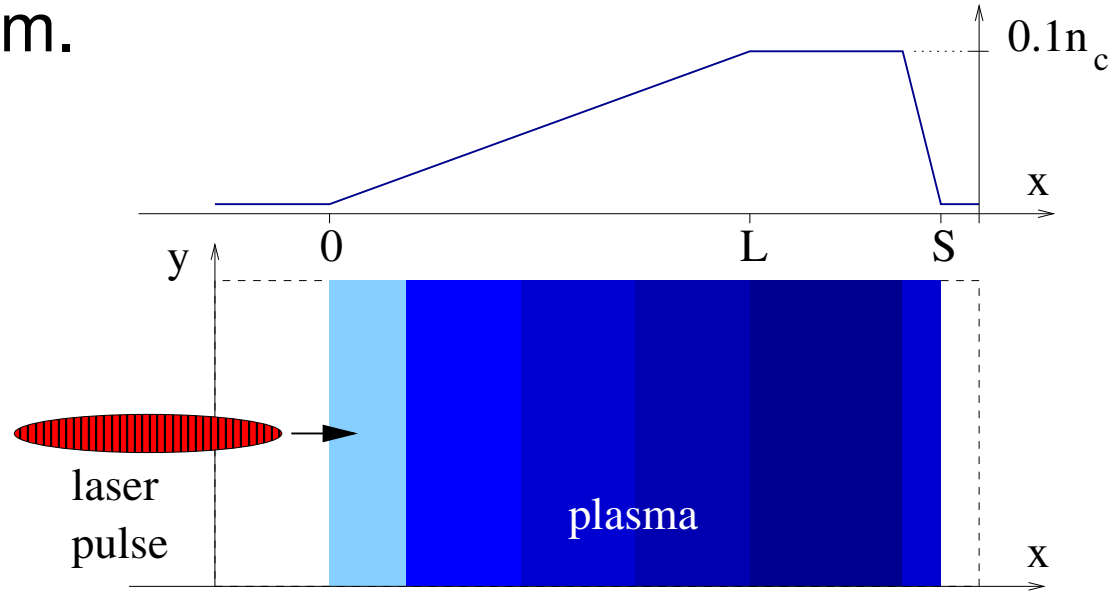

Variety of nonlinear effects

Variety of nonlinear effects

Top frame: laser field E_z
(scale magnified $\times 3$ for $50 < x/\lambda < 250$)
Bottom frame: ion density n_i

Variety of nonlinear effects

Top frame: laser field E_z
(scale magnified $\times 3$ for $50 < x/\lambda < 250$)
Bottom frame: ion density n_i

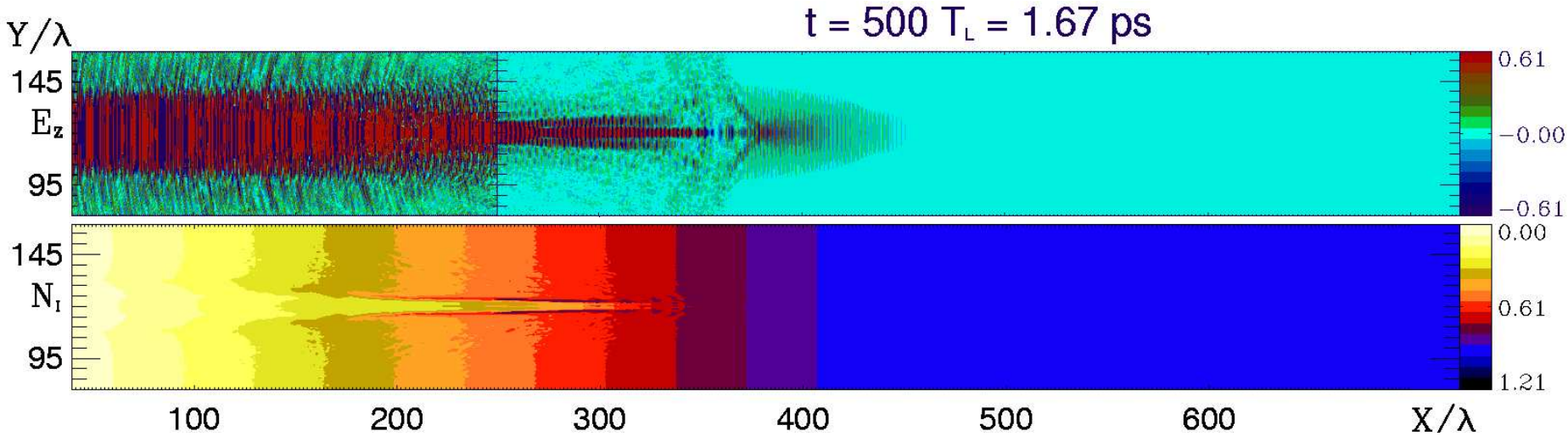

Variety of nonlinear effects

Top frame: laser field E_z
(scale magnified $\times 3$ for $50 < x/\lambda < 250$)
Bottom frame: ion density n_i

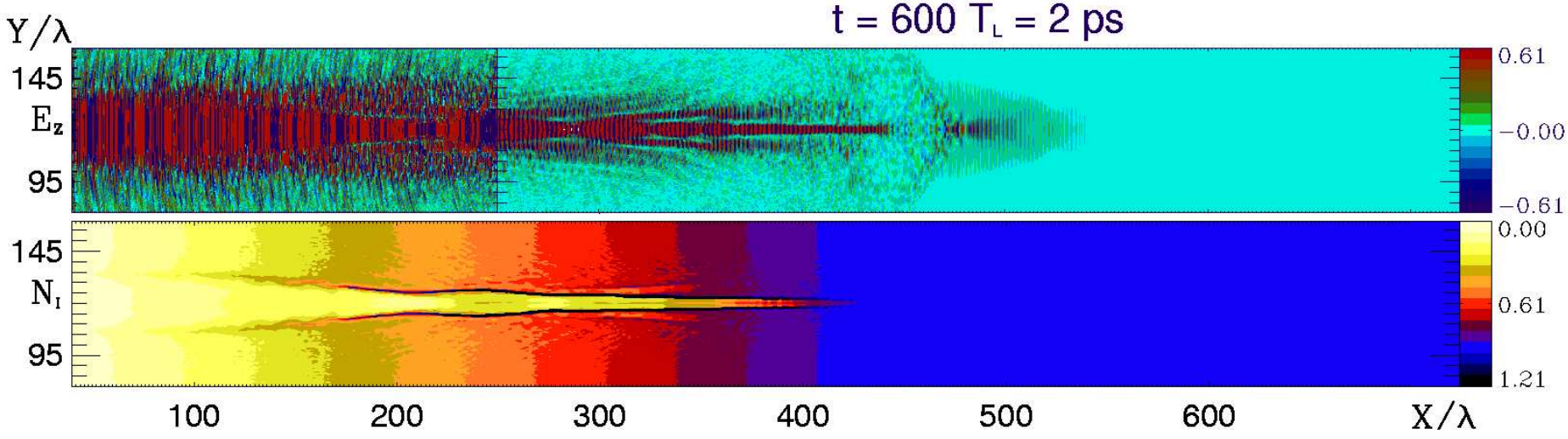

Variety of nonlinear effects

Top frame: laser field E_z
(scale magnified $\times 3$ for $50 < x/\lambda < 250$)
Bottom frame: ion density n_i

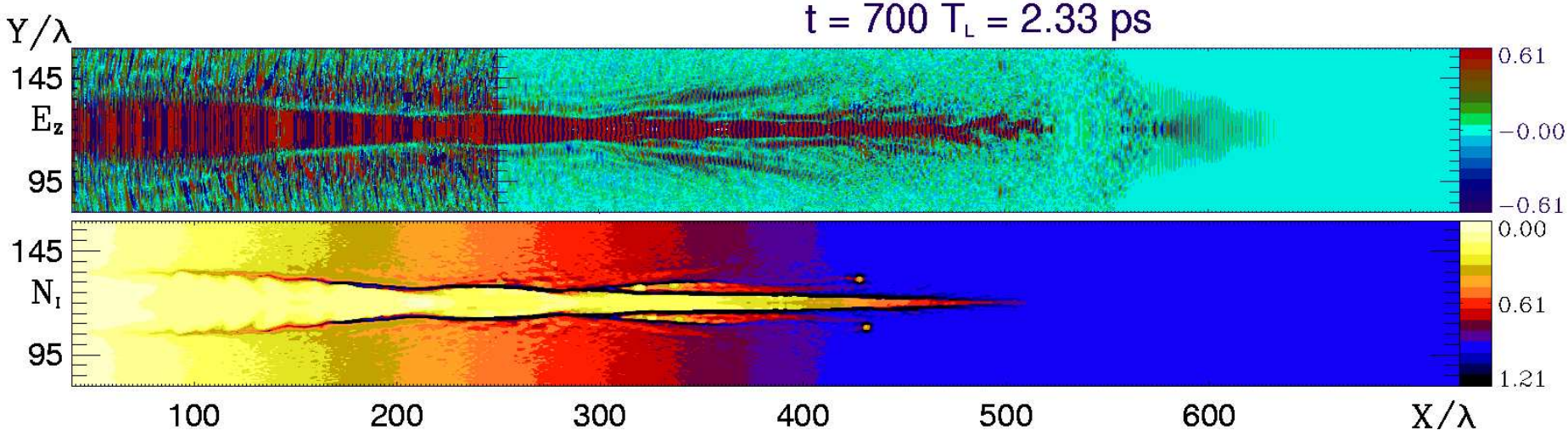

Variety of nonlinear effects

Top frame: laser field E_z
(scale magnified $\times 3$ for $50 < x/\lambda < 250$)
Bottom frame: ion density n_i

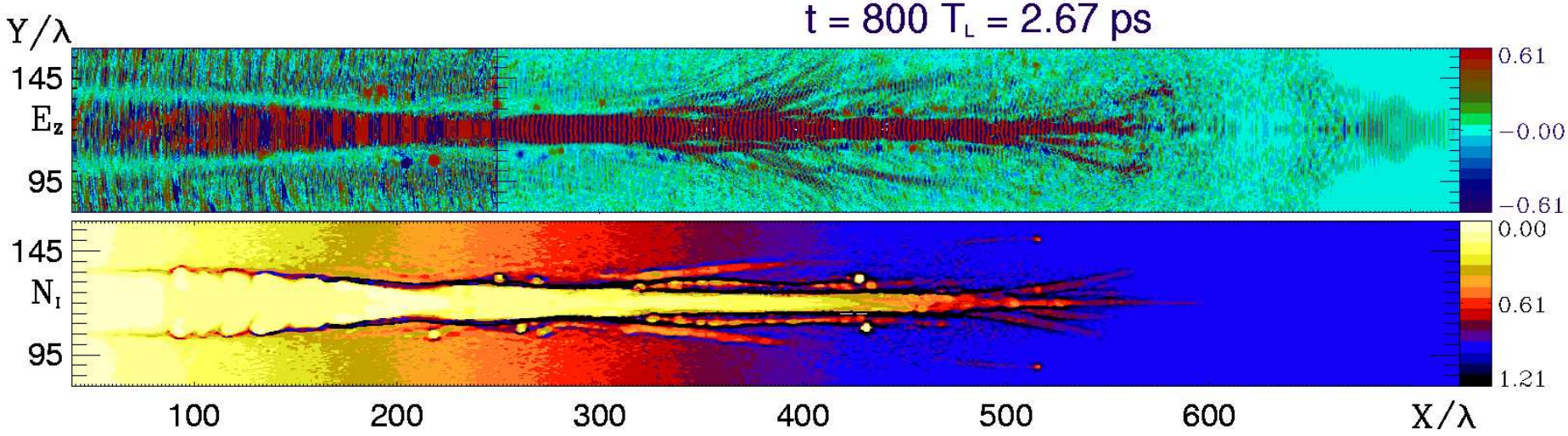

Variety of nonlinear effects

Top frame: laser field E_z
(scale magnified $\times 3$ for $50 < x/\lambda < 250$)
Bottom frame: ion density n_i

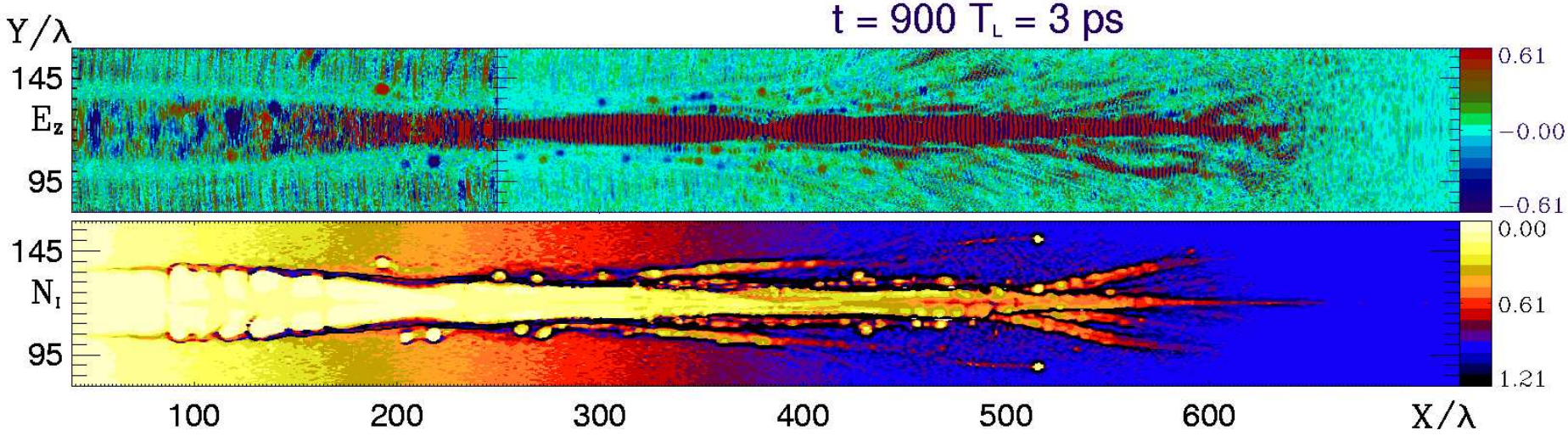

Variety of nonlinear effects

Top frame: laser field E_z
(scale magnified $\times 3$ for $50 < x/\lambda < 250$)
Bottom frame: ion density n_i

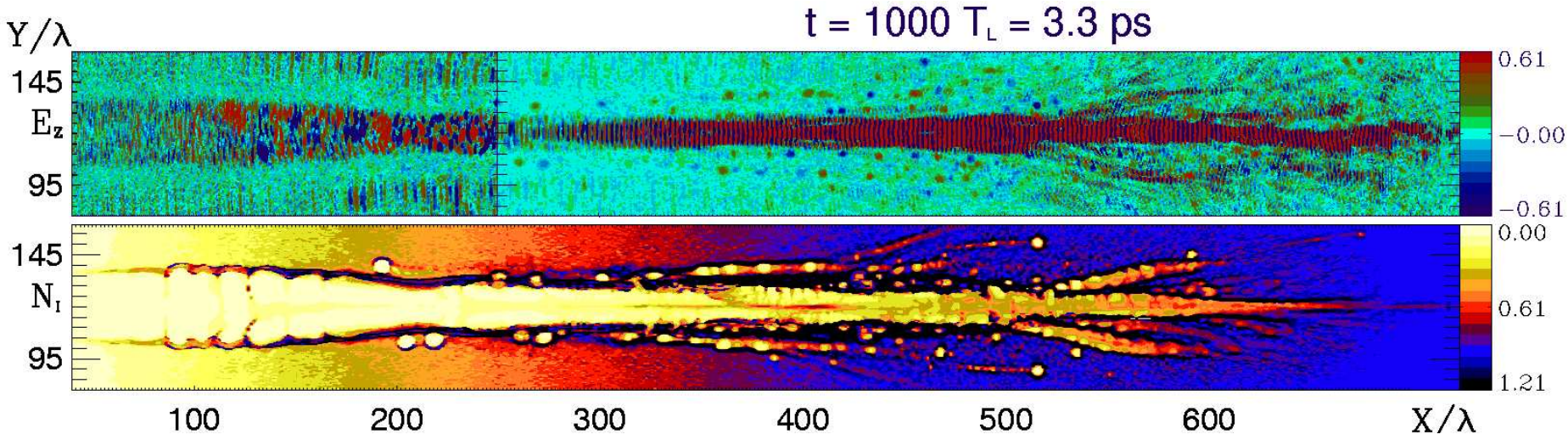

Variety of nonlinear effects

Top frame: laser field E_z
(scale magnified $\times 3$ for $50 < x/\lambda < 250$)
Bottom frame: ion density n_i

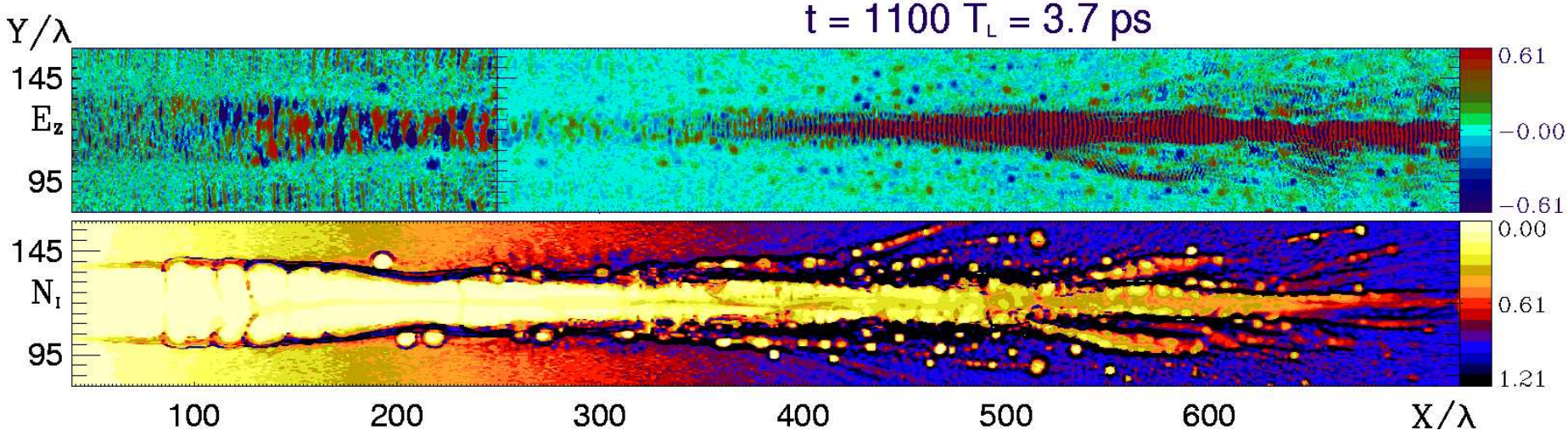

Variety of nonlinear effects

Top frame: laser field E_z
(scale magnified $\times 3$ for $50 < x/\lambda < 250$)
Bottom frame: ion density n_i

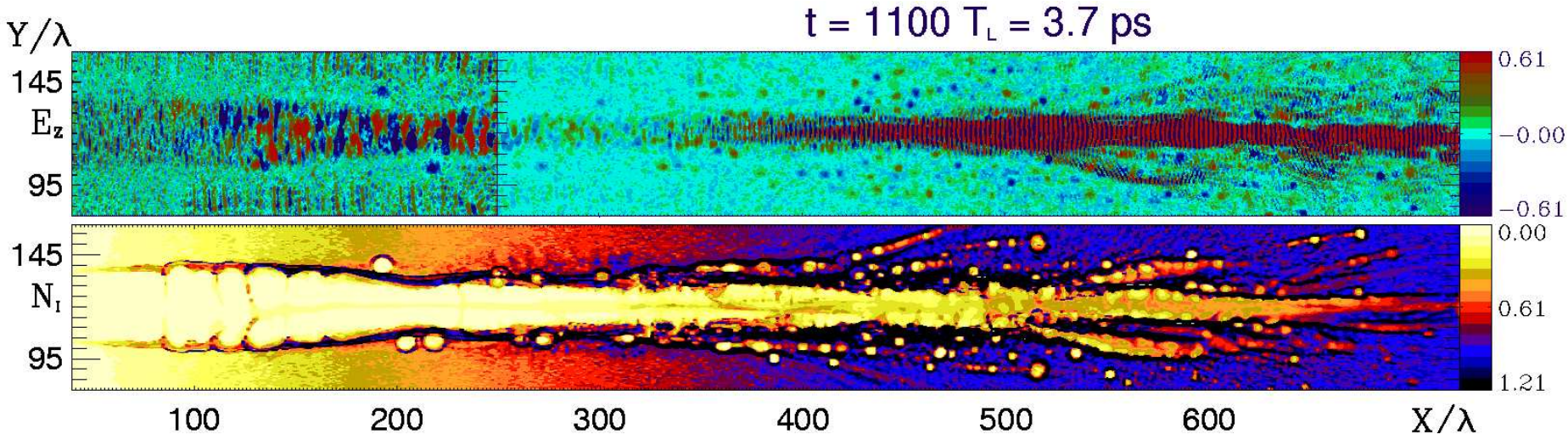

Channel boring, beam breakup, formation of “solitons”, quasi-regular patterns inside channels . . .

Self-channeling and radial field evolution

Self-channeling and radial field evolution

At moderate intensity $a_L = 1.7$ the laser pulse drills a regular charge-displacement channel in the low-density region

Self-channeling and radial field evolution

At moderate intensity $a_L = 1.7$ the laser pulse drills a regular charge-displacement channel in the low-density region

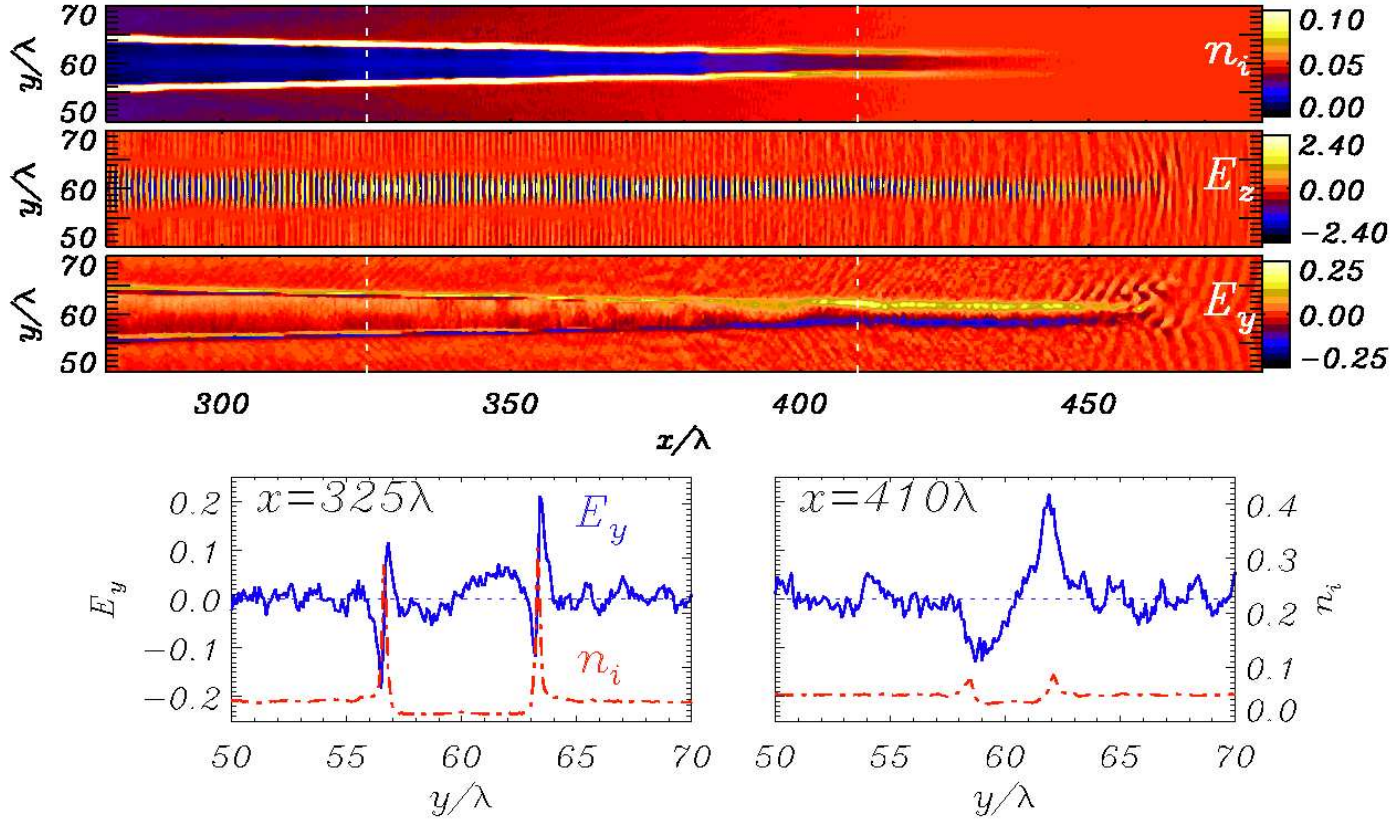

Self-channeling and radial field evolution

At moderate intensity $a_L = 1.7$ the laser pulse drills a regular charge-displacement channel in the low-density region

The "radial" space-charge field (E_y) changes its profile along the propagation direction

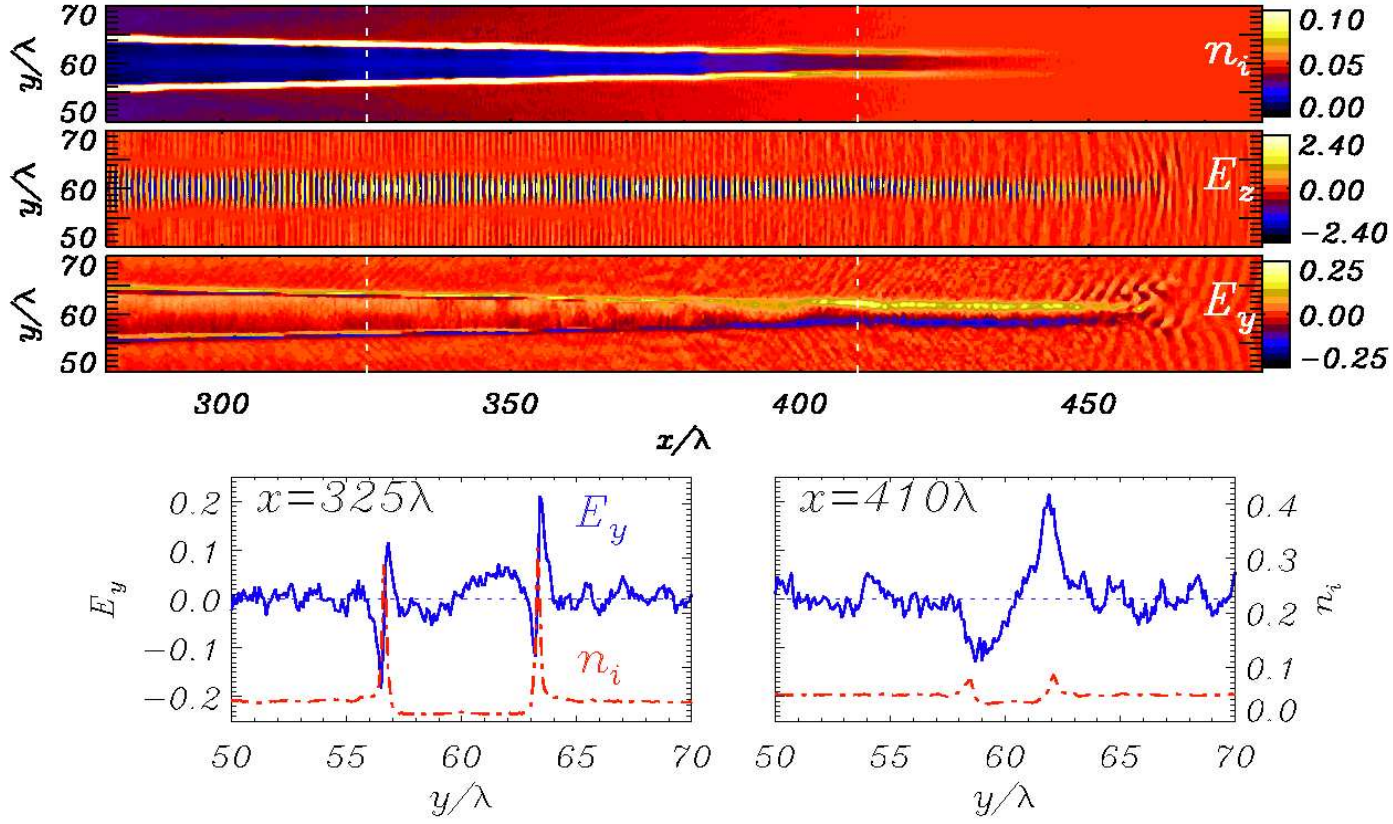

[S.Kar et al., arXiv:physics/0702177]

Ponderomotive electrostatic 1D model

Ponderomotive electrostatic 1D model

- 1D electrostatic PIC simulation, cylindrical geometry

Ponderomotive electrostatic 1D model

- 1D electrostatic PIC simulation, cylindrical geometry
- Laser pulse action is included via the radial ponderomotive force on electrons (as an “external” driver)

$$F_p = -m_e c^2 \nabla \sqrt{1 + a^2(r,t)/2}$$
$$a^2(r,t) = a_L^2 e^{-(r/r_0)^2 - (t/\tau)^2}$$

Ponderomotive electrostatic 1D model

- 1D electrostatic PIC simulation, cylindrical geometry
- Laser pulse action is included via the radial ponderomotive force on electrons (as an "external" driver)

$$F_p = -m_e c^2 \nabla \sqrt{1 + a^2(r,t)/2}$$
$$a^2(r,t) = a_L^2 e^{-(r/r_0)^2 - (t/\tau)^2}$$

- Model equations

$$\frac{dp_e}{dt} = -eE_r + F_p, \qquad \frac{dp_i}{dt} = ZeE_r$$
$$\frac{1}{r}\frac{\partial}{\partial r}(rE_r) = 4\pi\rho = e(Zn_i - n_e).$$

Ponderomotive electrostatic 1D model

- 1D electrostatic PIC simulation, cylindrical geometry
- Laser pulse action is included via the radial ponderomotive force on electrons (as an "external" driver)

$$F_p = -m_e c^2 \nabla \sqrt{1 + a^2(r,t)/2}$$
$$a^2(r,t) = a_L^2 e^{-(r/r_0)^2 - (t/\tau)^2}$$

- Model equations

$$\frac{dp_e}{dt} = -eE_r + F_p, \qquad \frac{dp_i}{dt} = ZeE_r$$
$$\frac{1}{r}\frac{\partial}{\partial r}(rE_r) = 4\pi\rho = e(Zn_i - n_e).$$

[A. Macchi et al, arXiv:physics/0701139]

Echo effect in the radial field

Echo effect in the radial field

1D electrostatic PIC simulation

$a_L = 2.7$, $\tau_L = 300 T_L$, $r_L = 7.5\lambda$

Echo effect in the radial field

1D electrostatic PIC simulation

$a_L = 2.7$, $\tau_L = 300 T_L$, $r_L = 7.5\lambda$

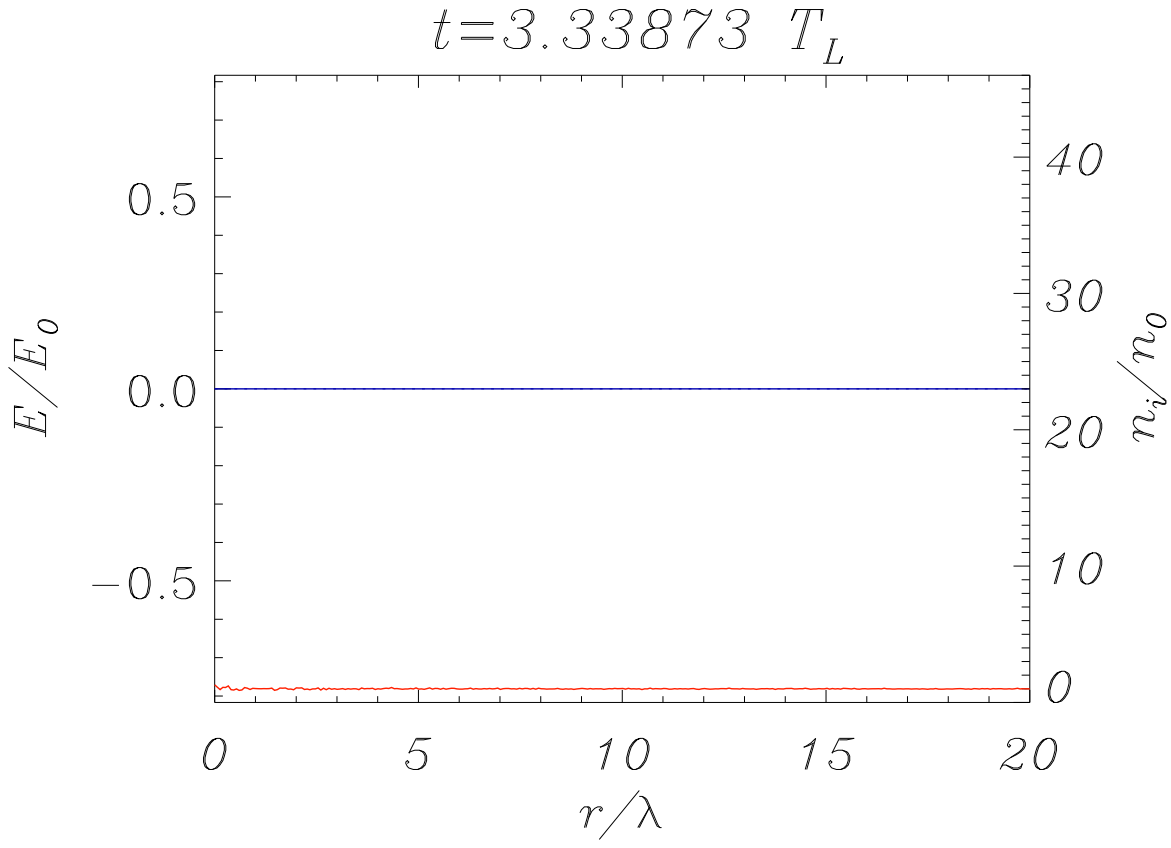

During the laser pulse the space-charge field E_r created by electron depletion in the channel exactly balances the PM force F_p

Echo effect in the radial field

1D electrostatic PIC simulation

$a_L = 2.7$, $\tau_L = 300 T_L$, $r_L = 7.5\lambda$

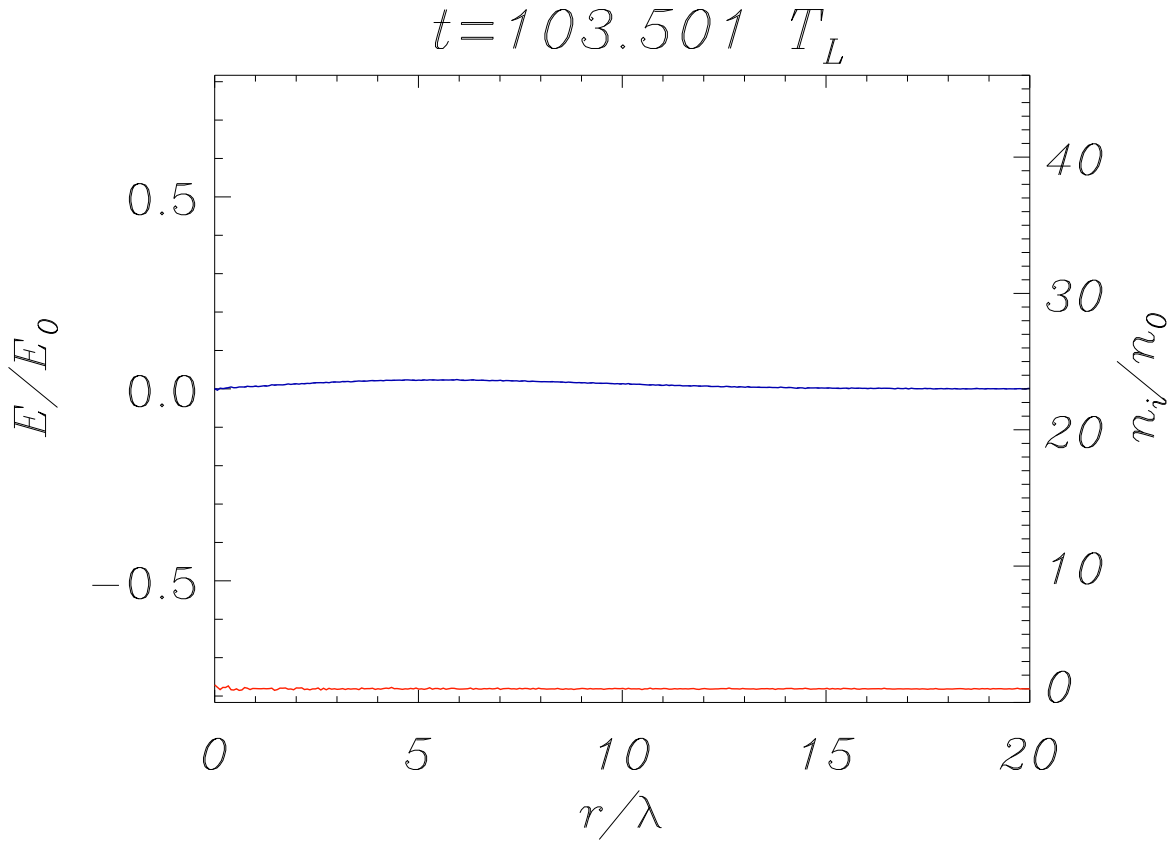

During the laser pulse the space-charge field E_r created by electron depletion in the channel exactly balances the PM force F_p

Echo effect in the radial field

1D electrostatic PIC simulation

$a_L = 2.7$, $\tau_L = 300 T_L$, $r_L = 7.5\lambda$

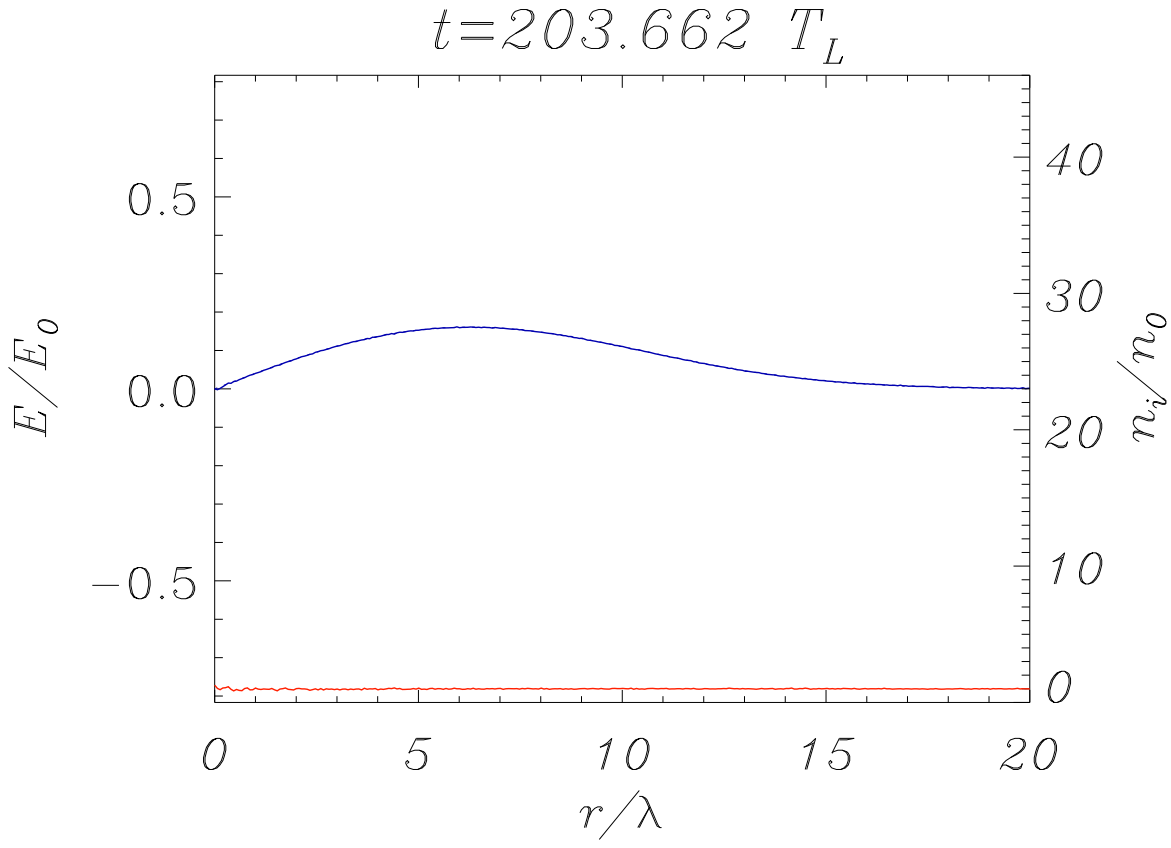

During the laser pulse the space-charge field E_r created by electron depletion in the channel exactly balances the PM force F_p

Echo effect in the radial field

1D electrostatic PIC simulation

$a_L = 2.7$, $\tau_L = 300 T_L$, $r_L = 7.5\lambda$

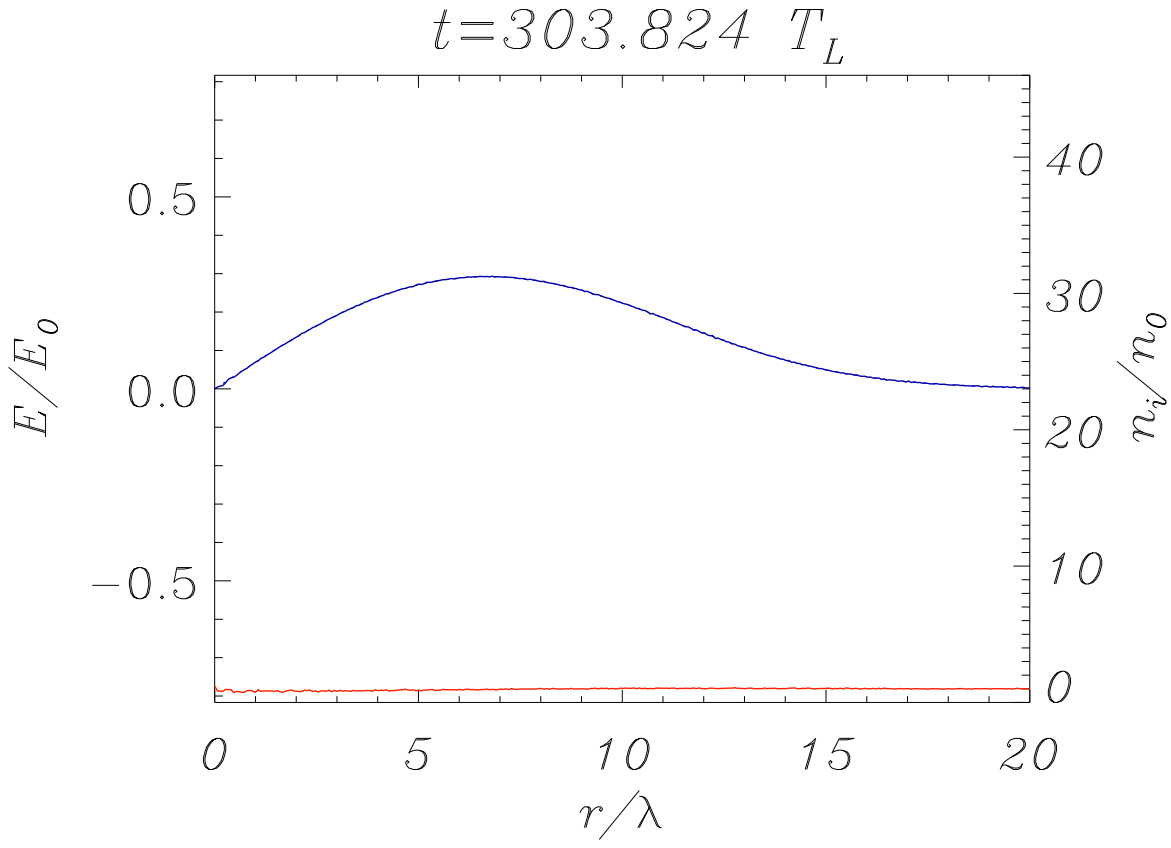

During the laser pulse the space-charge field E_r created by electron depletion in the channel exactly balances the PM force F_p

Echo effect in the radial field

1D electrostatic PIC simulation

$a_L = 2.7$, $\tau_L = 300 T_L$, $r_L = 7.5\lambda$

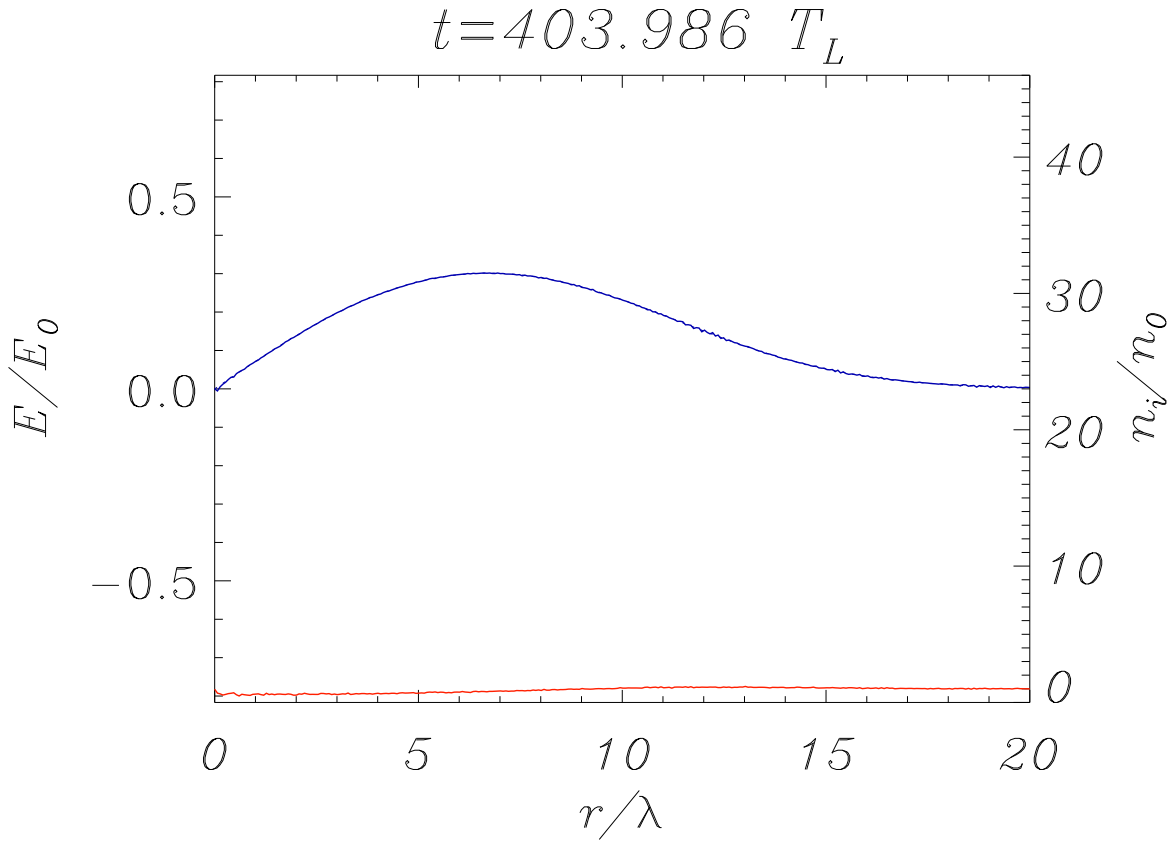

During the laser pulse the space-charge field E_r created by electron depletion in the channel exactly balances the PM force F_p

Echo effect in the radial field

1D electrostatic PIC simulation

$a_L = 2.7$, $\tau_L = 300 T_L$, $r_L = 7.5\lambda$

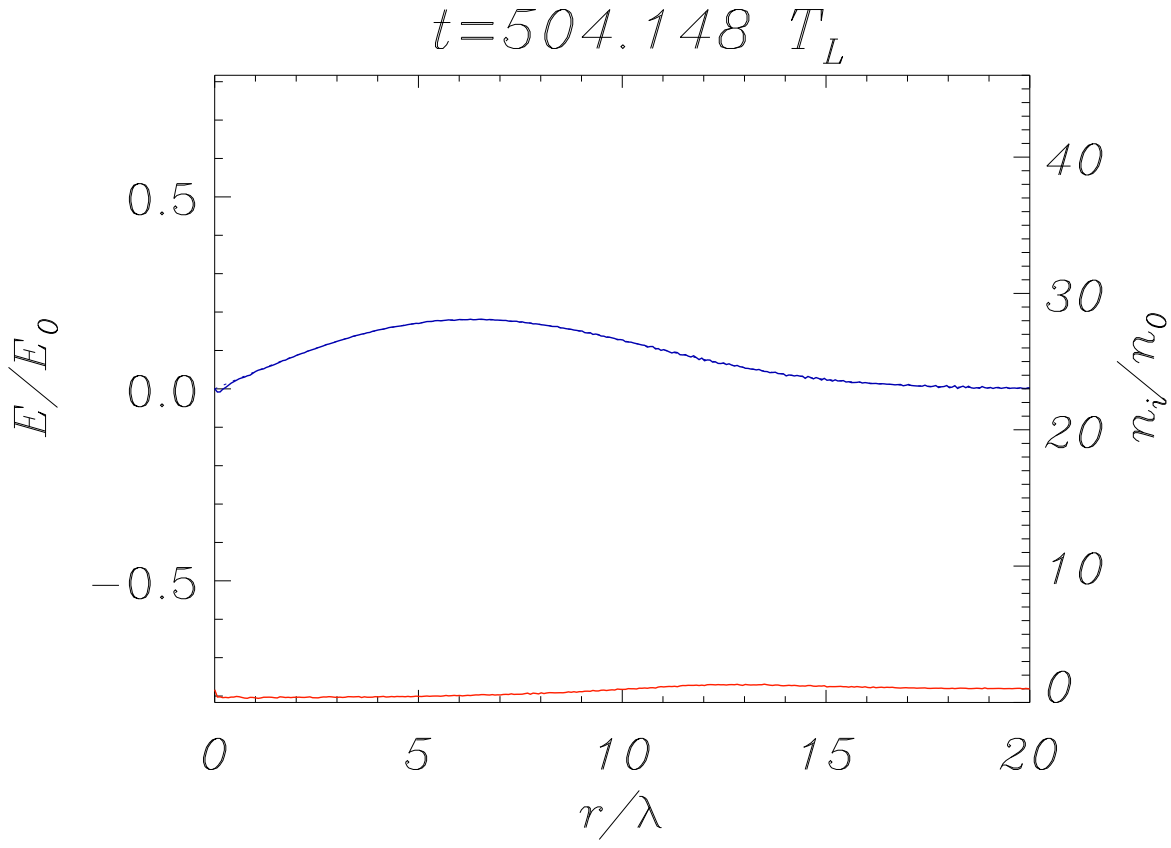

During the laser pulse the space-charge field E_r created by electron depletion in the channel exactly balances the PM force F_p

Echo effect in the radial field

1D electrostatic PIC simulation

$a_L = 2.7$, $\tau_L = 300 T_L$, $r_L = 7.5\lambda$

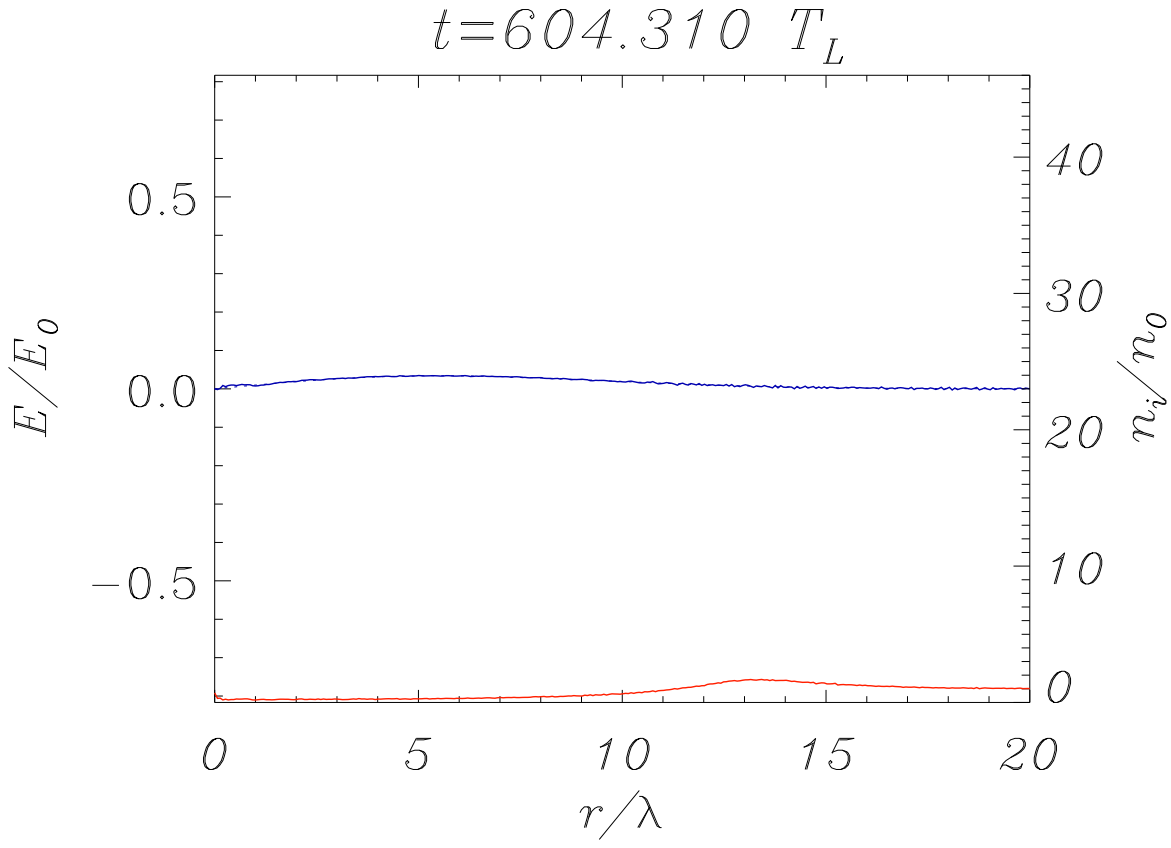

During the laser pulse the space-charge field E_r created by electron depletion in the channel exactly balances the PM force F_p

Echo effect in the radial field

1D electrostatic PIC simulation

$a_L = 2.7$, $\tau_L = 300 T_L$, $r_L = 7.5\lambda$

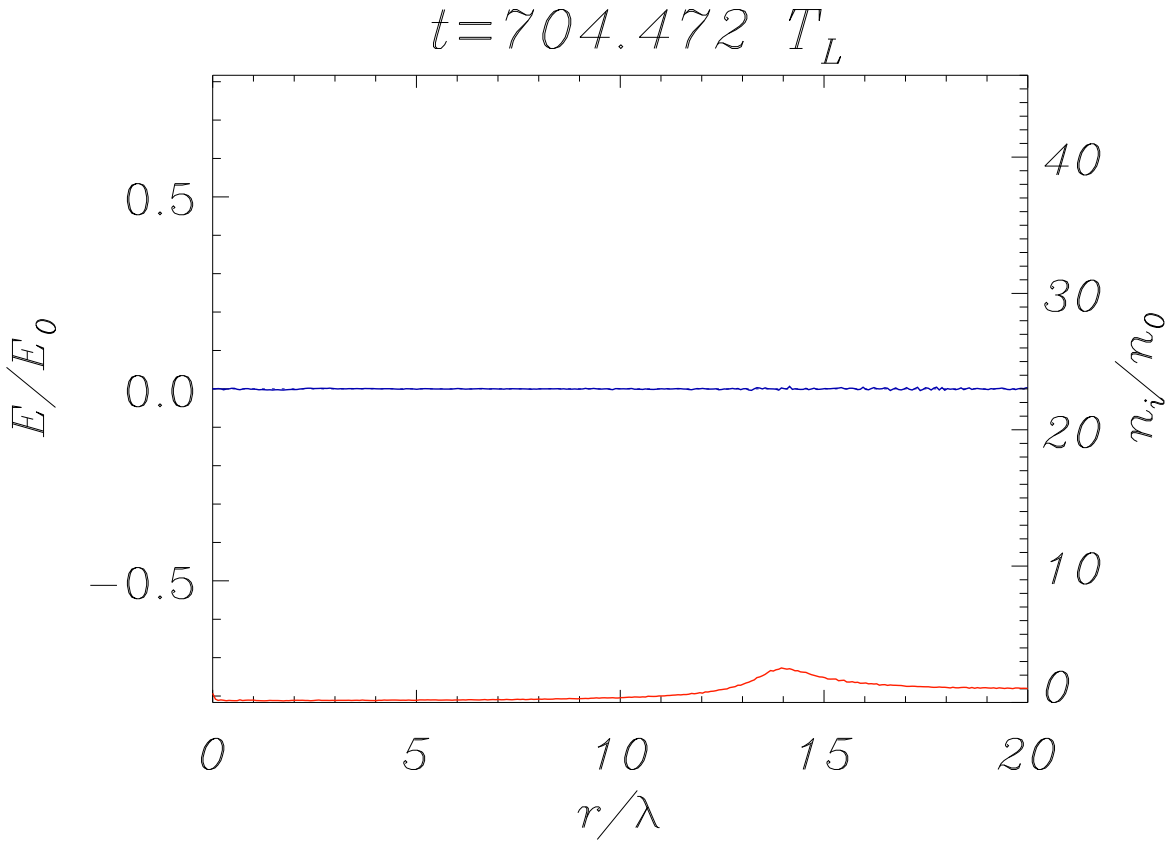

After the laser pulse E_r has almost vanished

Echo effect in the radial field

1D electrostatic PIC simulation

$a_L = 2.7$, $\tau_L = 300 T_L$, $r_L = 7.5\lambda$

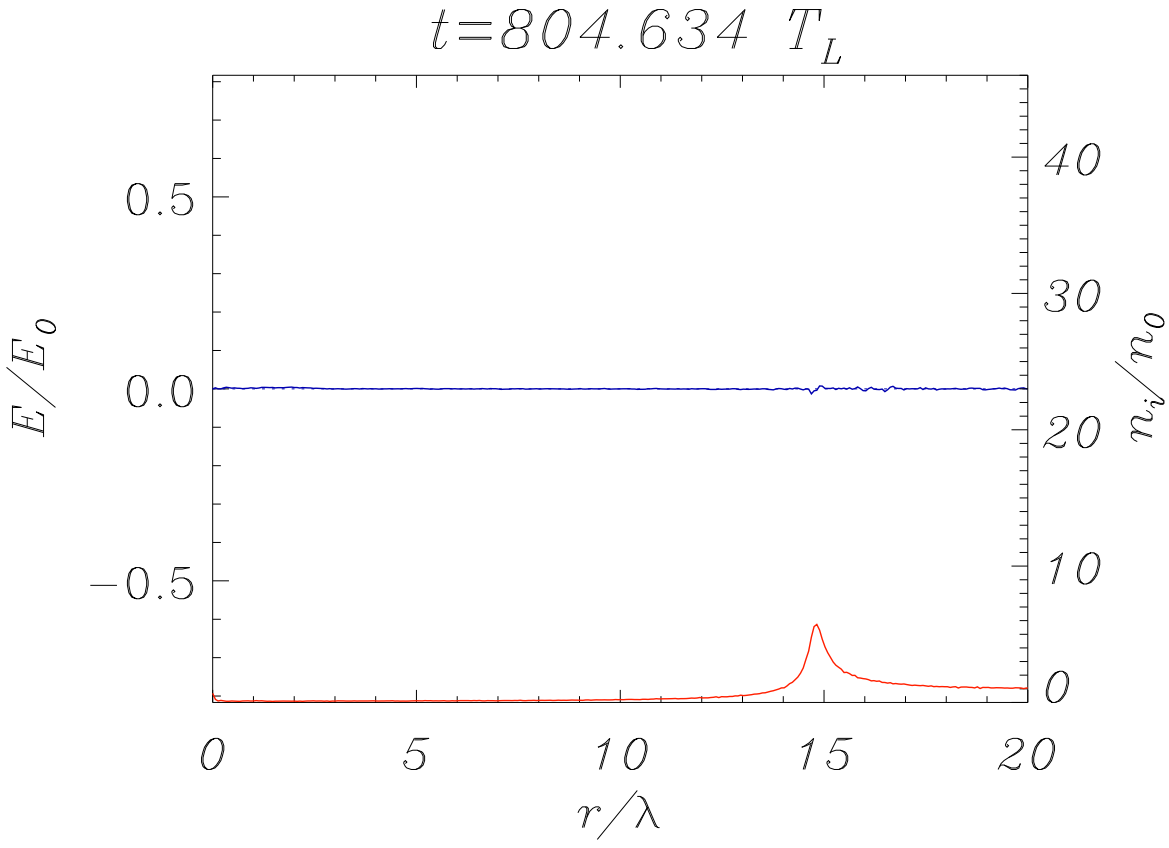

After the laser pulse E_r has almost vanished

Echo effect in the radial field

1D electrostatic PIC simulation

$a_L = 2.7$, $\tau_L = 300 T_L$, $r_L = 7.5\lambda$

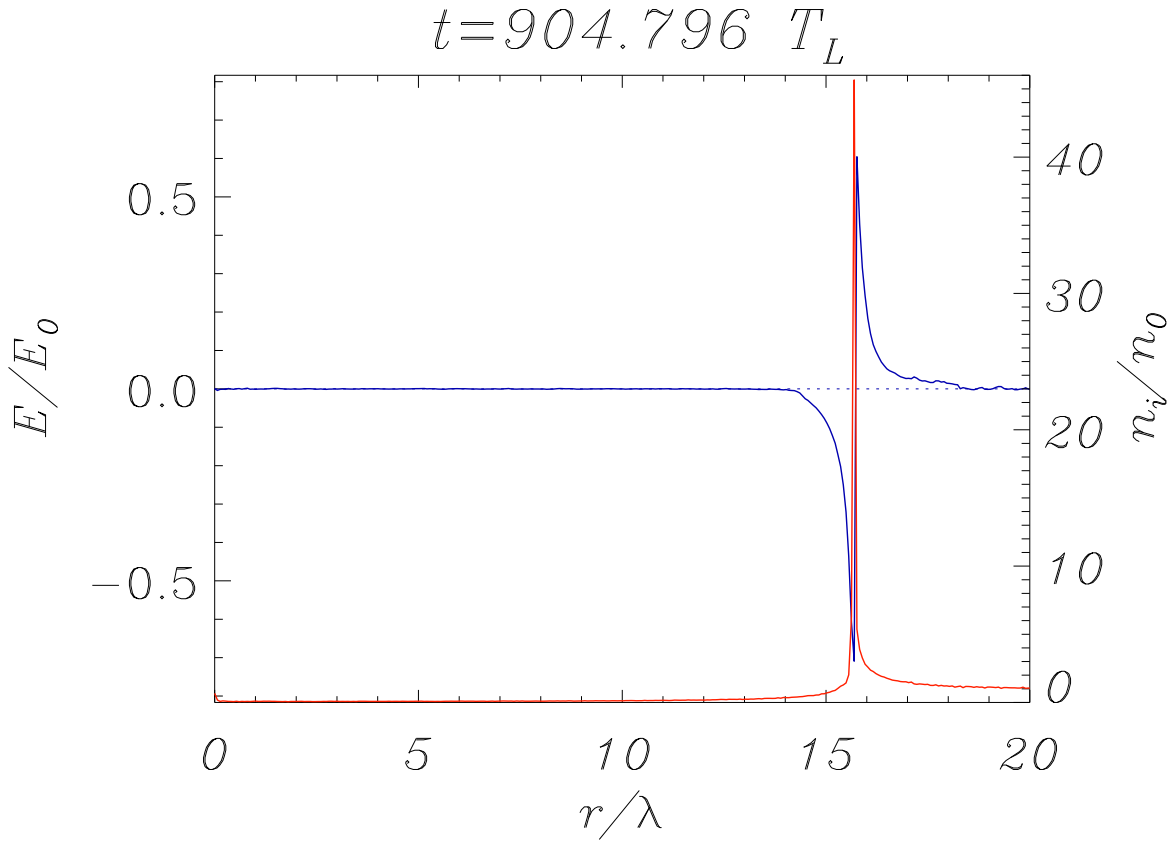

E_r appears back ("echo") where a sharp spike of n_i is produced;
the spike then "breaks" producing a fast bunch

Echo effect in the radial field

1D electrostatic PIC simulation

$a_L = 2.7$, $\tau_L = 300 T_L$, $r_L = 7.5\lambda$

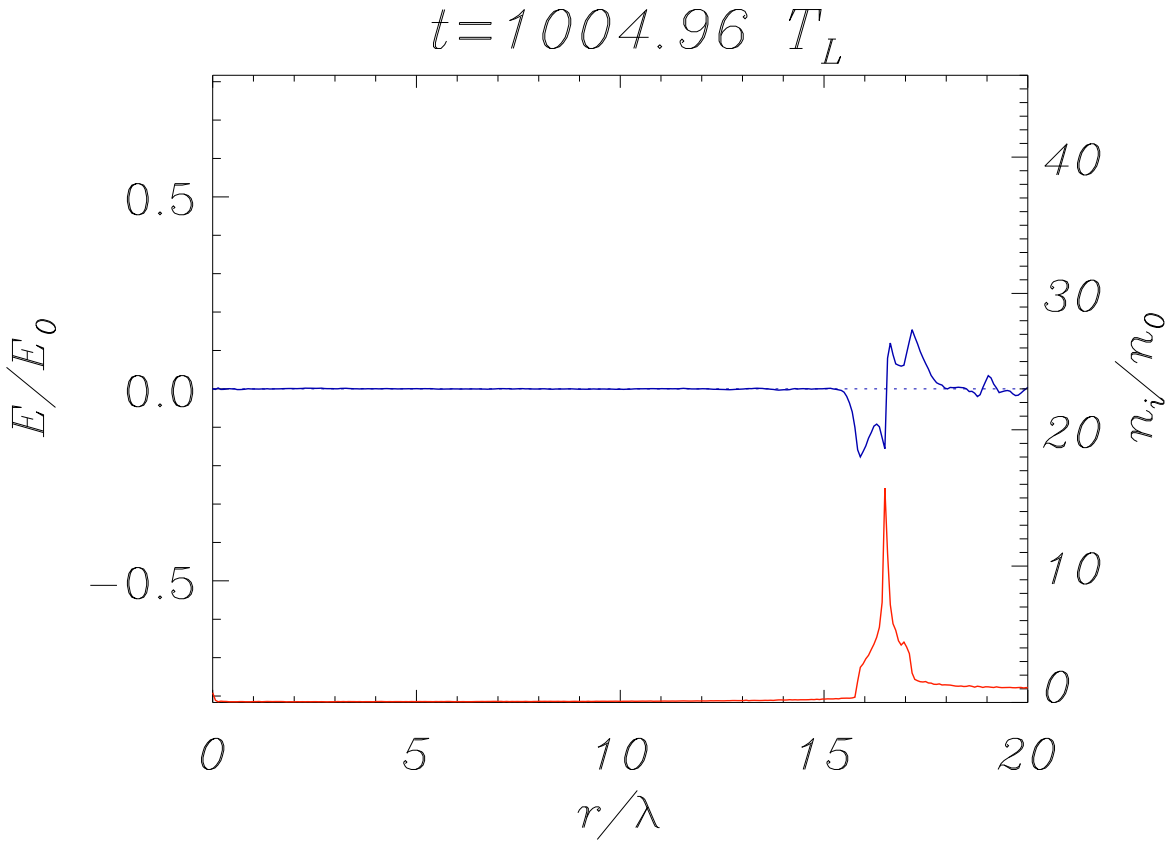

E_r appears back ("echo") where a sharp spike of n_i is produced;
the spike then "breaks" producing a fast bunch

Echo effect in the radial field

1D electrostatic PIC simulation

$a_L = 2.7$, $\tau_L = 300 T_L$, $r_L = 7.5\lambda$

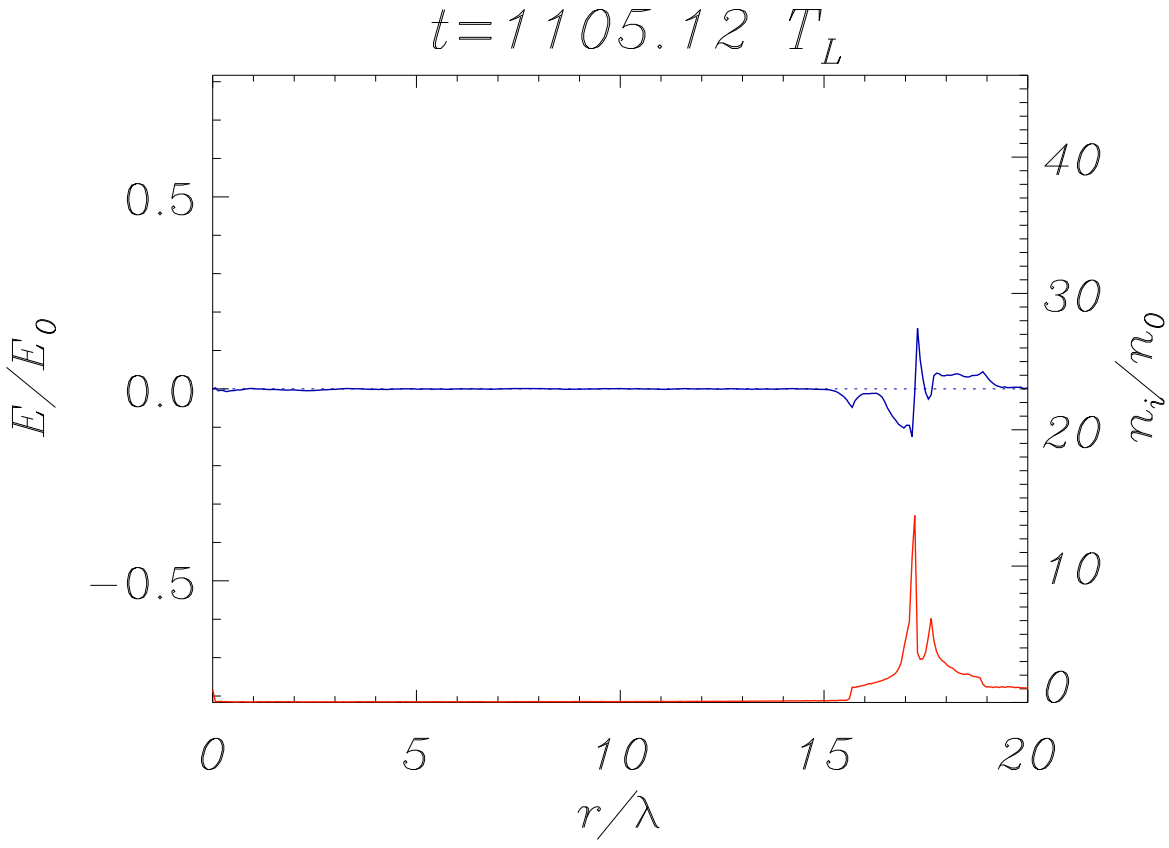

E_r appears back ("echo") where a sharp spike of n_i is produced;
the spike then "breaks" producing a fast bunch

Echo effect in the radial field

1D electrostatic PIC simulation

$a_L = 2.7$, $\tau_L = 300 T_L$, $r_L = 7.5\lambda$

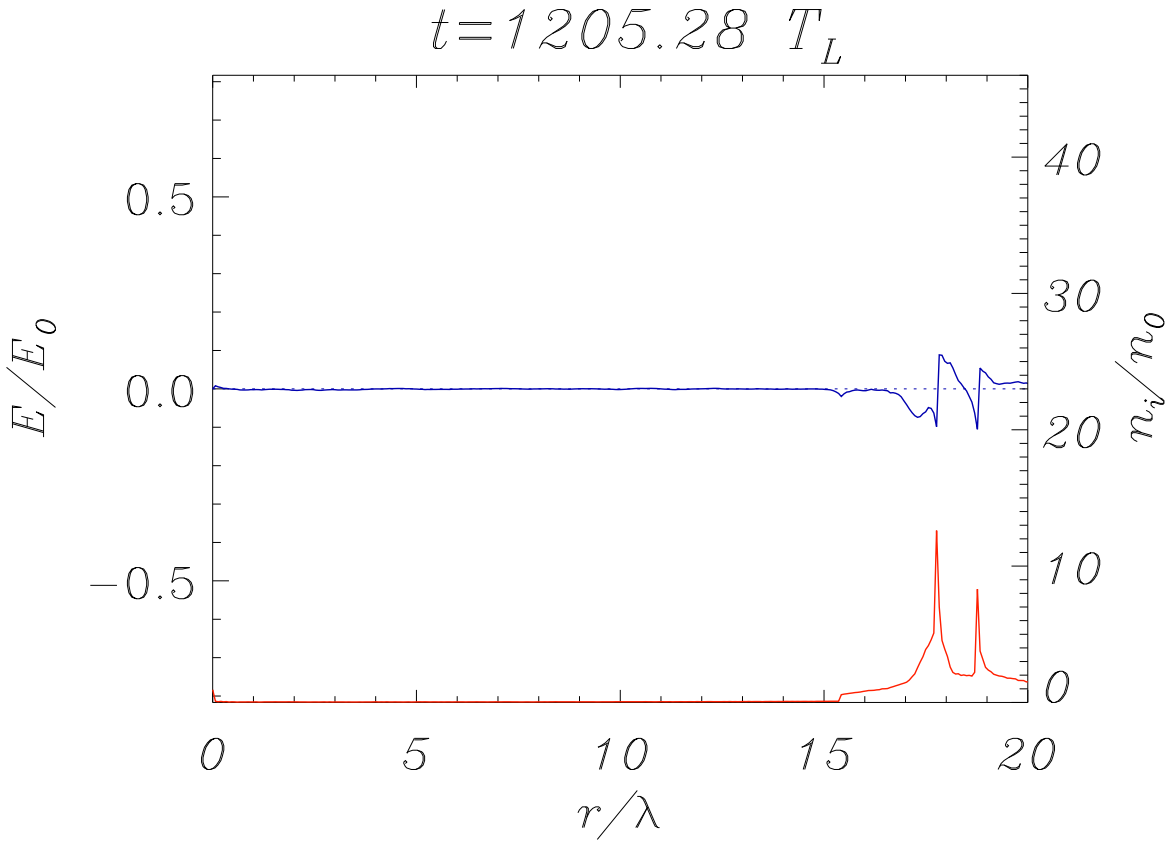

E_r appears back ("echo") where a sharp spike of n_i is produced;
the spike then "breaks" producing a fast bunch

Echo effect in the radial field

1D electrostatic PIC simulation

$a_L = 2.7$, $\tau_L = 300 T_L$, $r_L = 7.5\lambda$

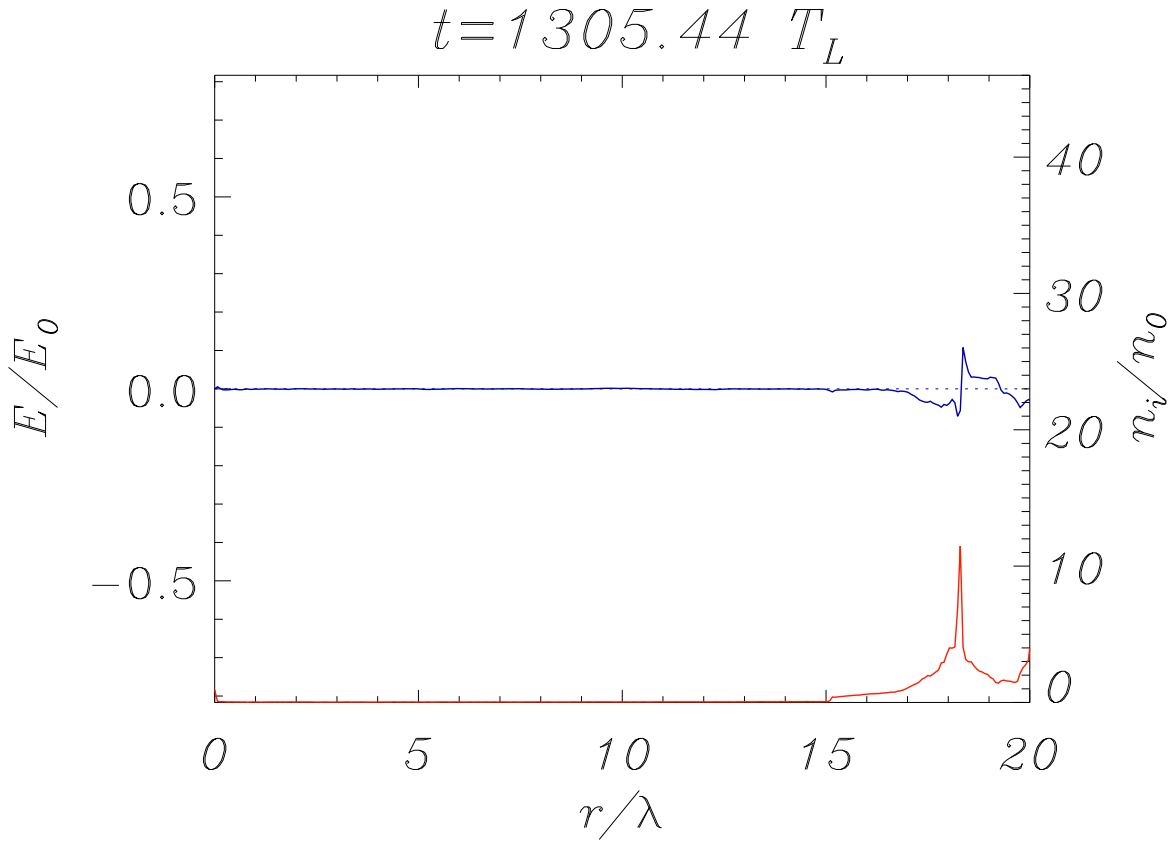

E_r appears back ("echo") where a sharp spike of n_i is produced;
the spike then "breaks" producing a fast bunch

Echo effect is due to “breaking”

Echo effect is due to “breaking”

Analysis of ion phase space show that hydrodynamical breaking occurs when faster ions overlap the slowest ones

Echo effect is due to “breaking”

Analysis of ion phase space show that hydrodynamical breaking occurs when faster ions overlap the slowest ones

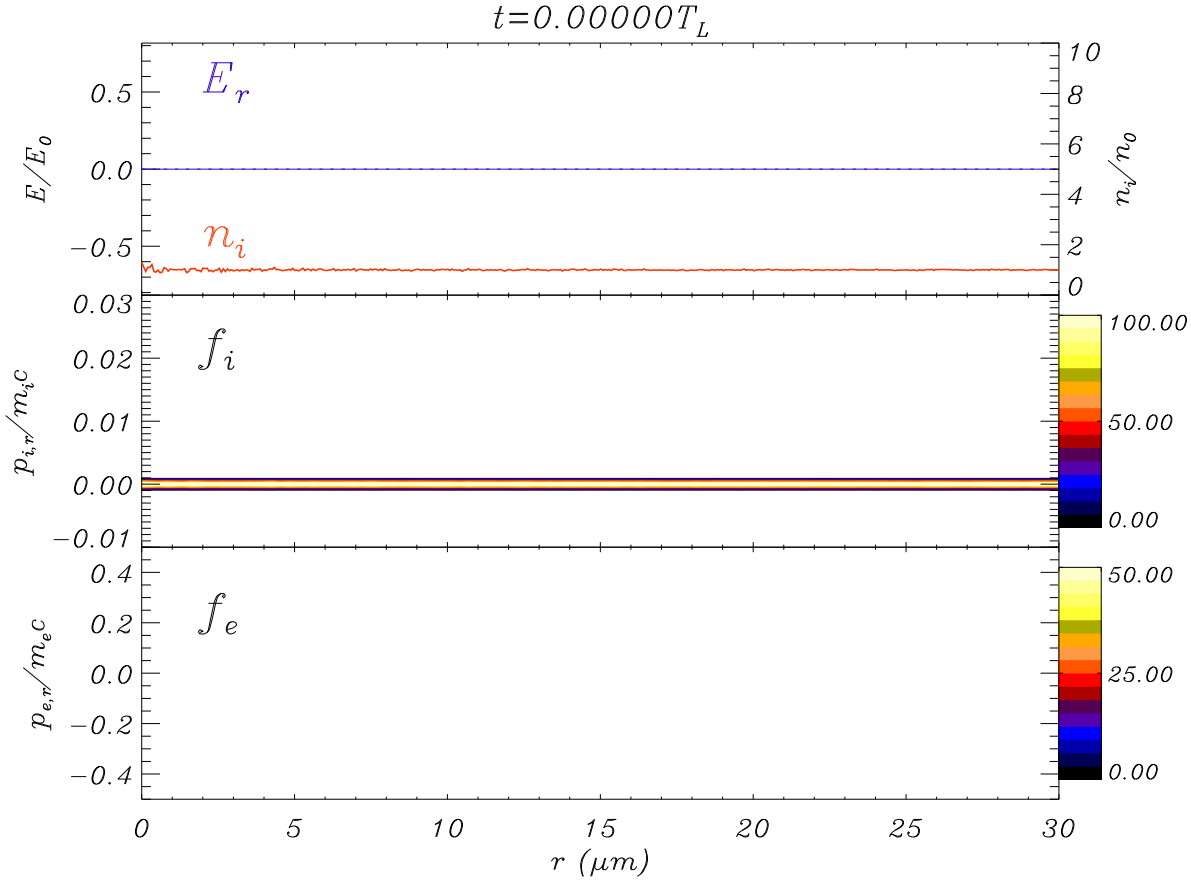

Echo effect is due to “breaking”

Analysis of ion phase space show that hydrodynamical breaking occurs when faster ions overlap the slowest ones

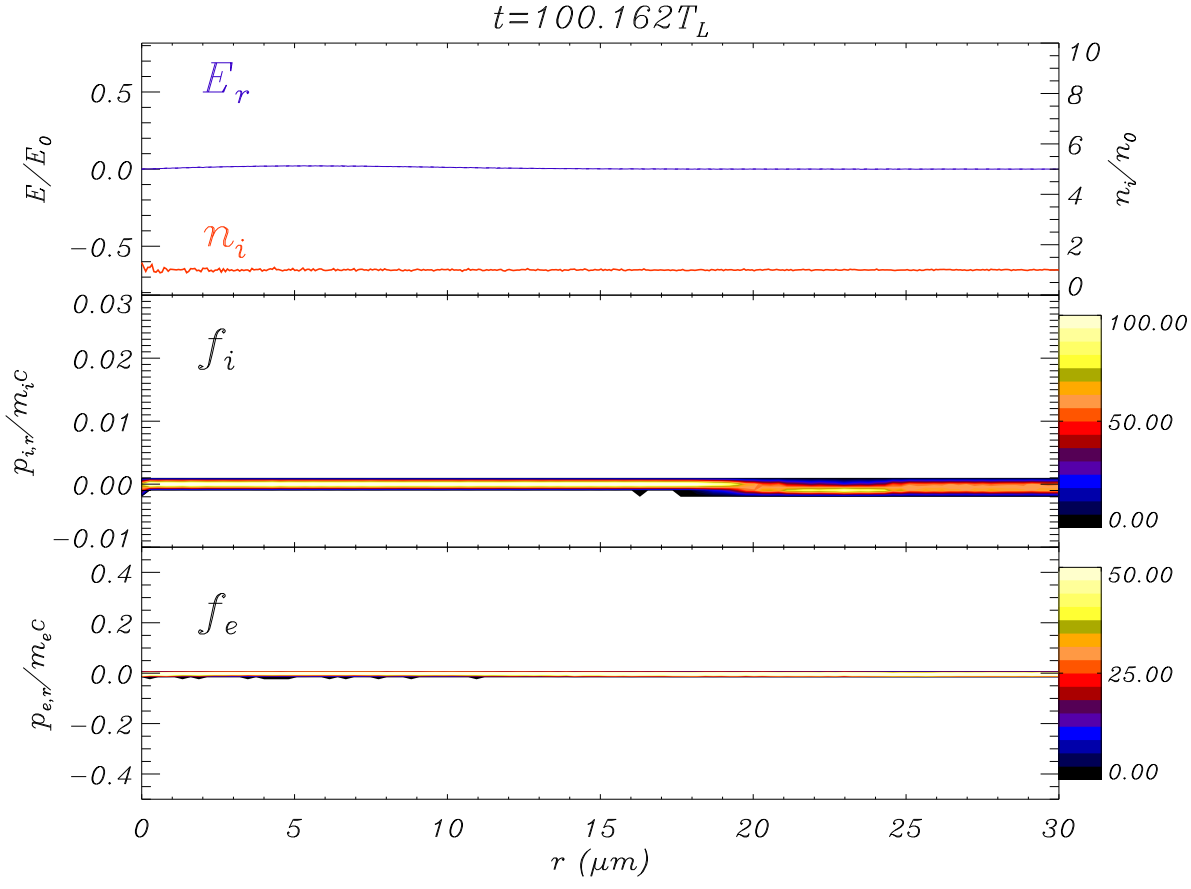

Echo effect is due to “breaking”

Analysis of ion phase space show that hydrodynamical breaking occurs when faster ions overlap the slowest ones

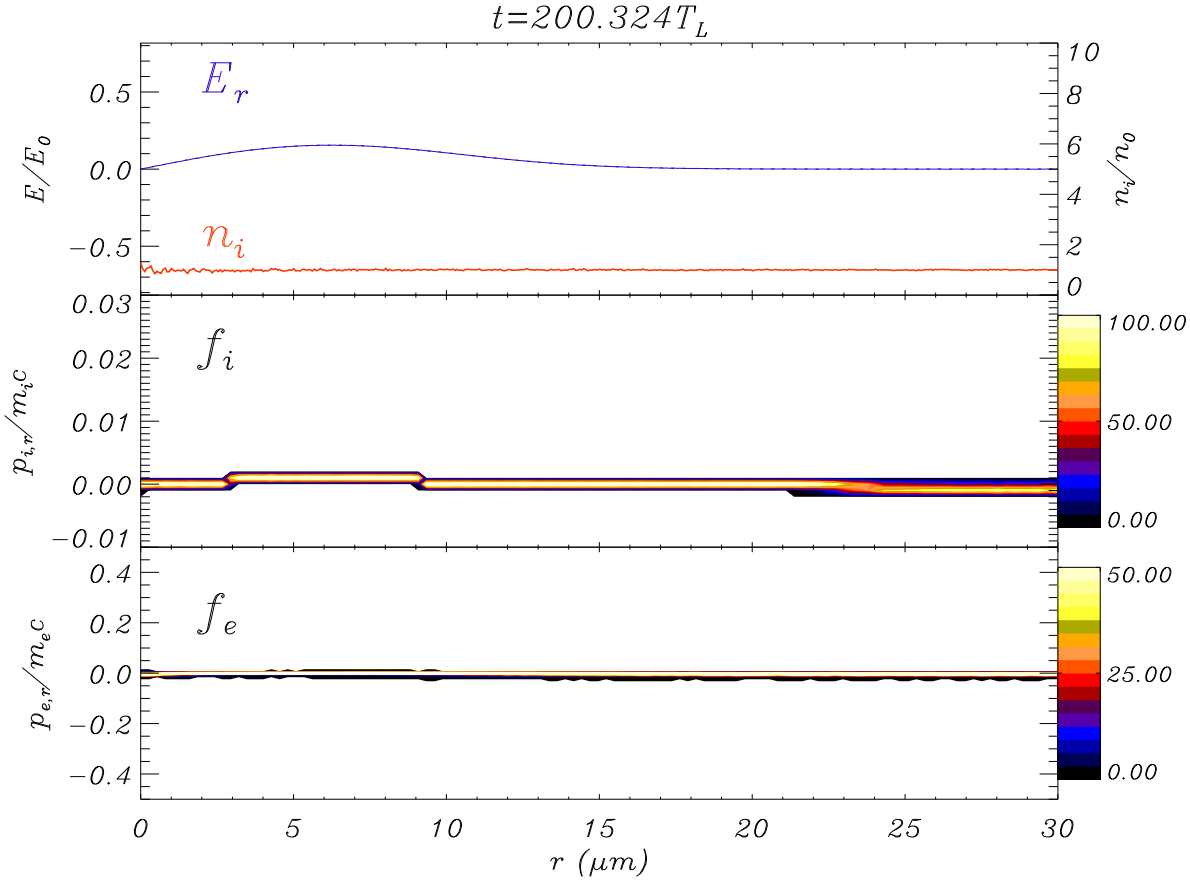

Echo effect is due to “breaking”

Analysis of ion phase space show that hydrodynamical breaking occurs when faster ions overlap the slowest ones

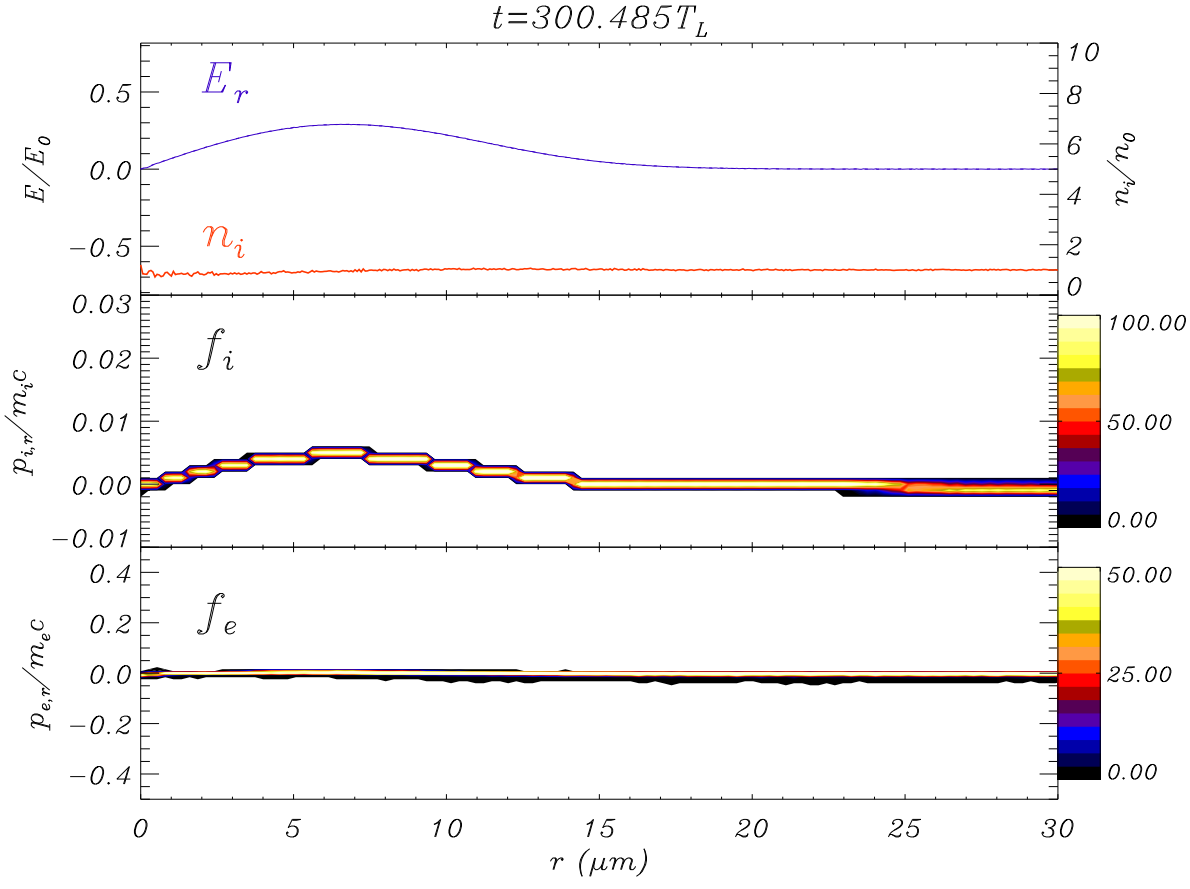

Echo effect is due to “breaking”

Analysis of ion phase space show that hydrodynamical breaking occurs when faster ions overlap the slowest ones

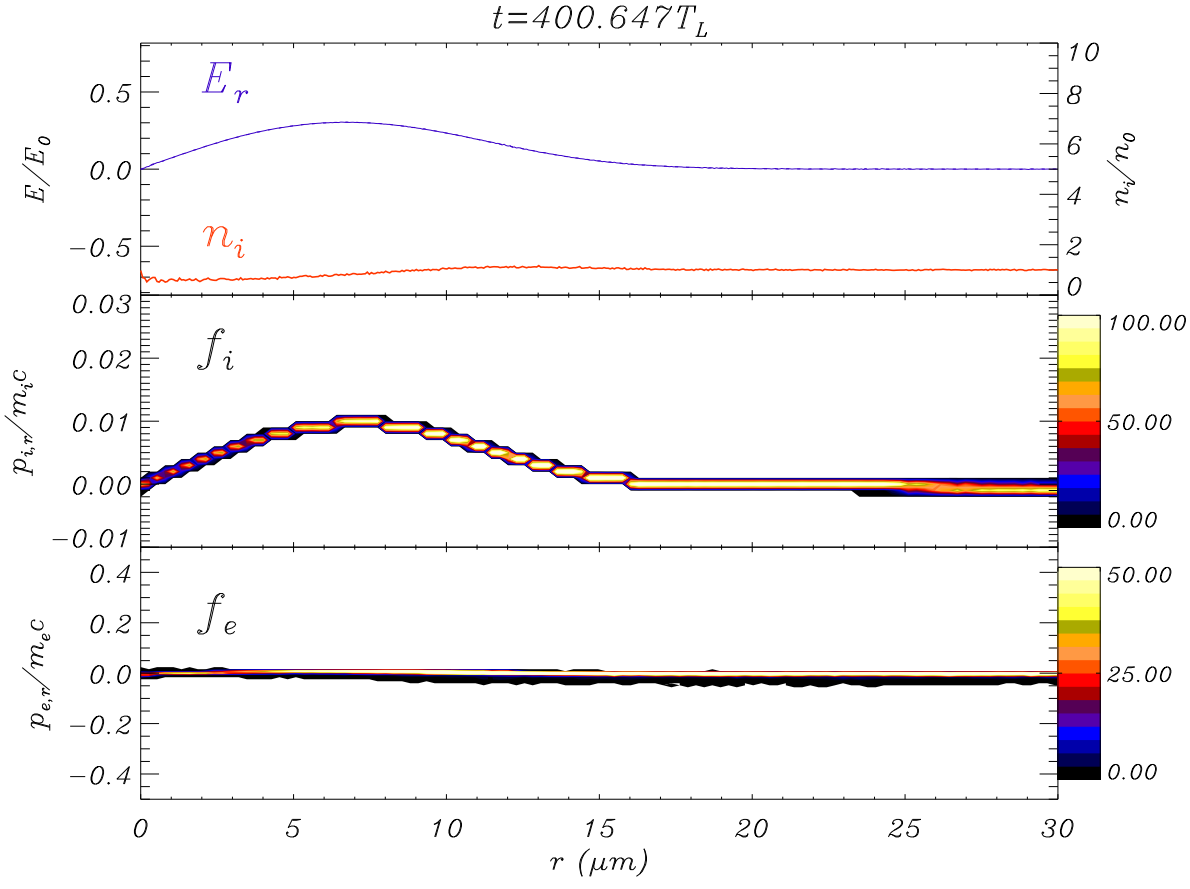

Echo effect is due to “breaking”

Analysis of ion phase space show that hydrodynamical breaking occurs when faster ions overlap the slowest ones

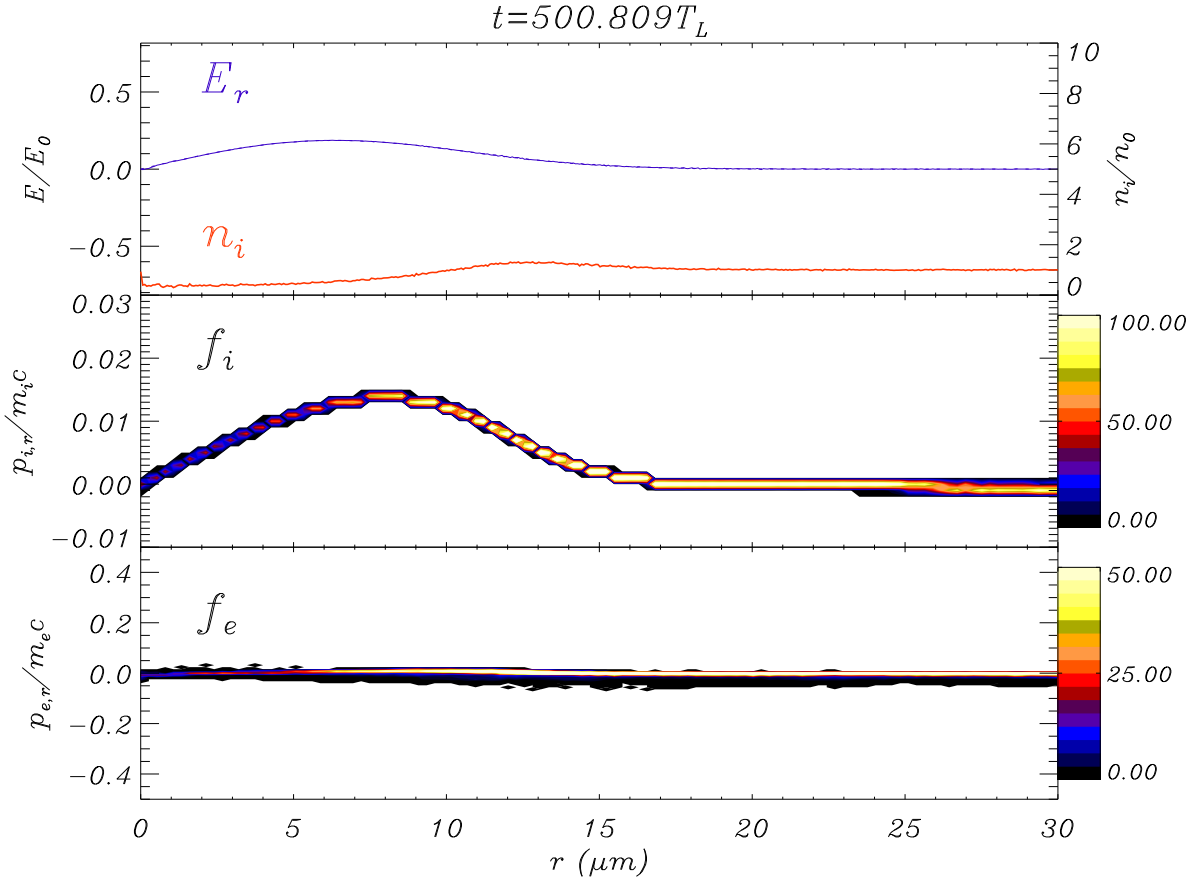

Echo effect is due to “breaking”

Analysis of ion phase space show that hydrodynamical breaking occurs when faster ions overlap the slowest ones

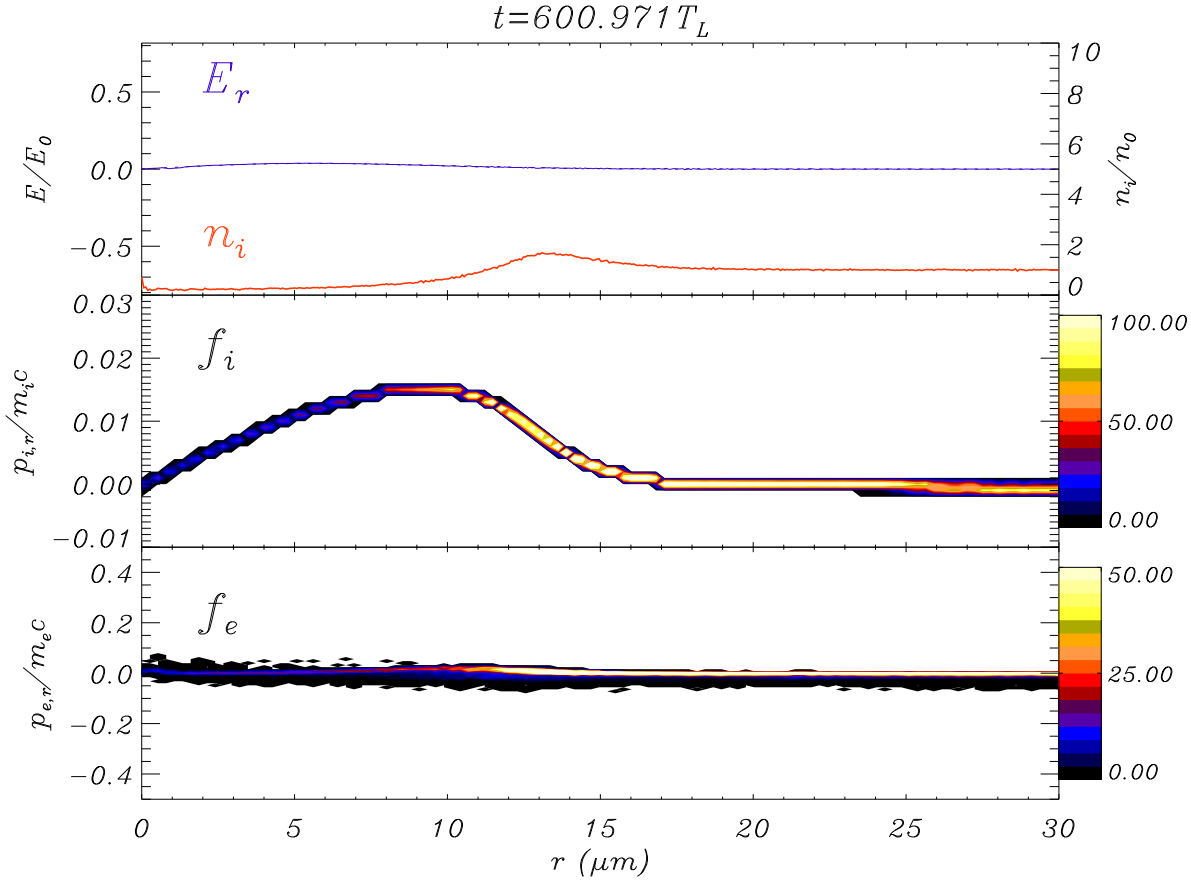

Echo effect is due to “breaking”

Analysis of ion phase space show that hydrodynamical breaking occurs when faster ions overlap the slowest ones

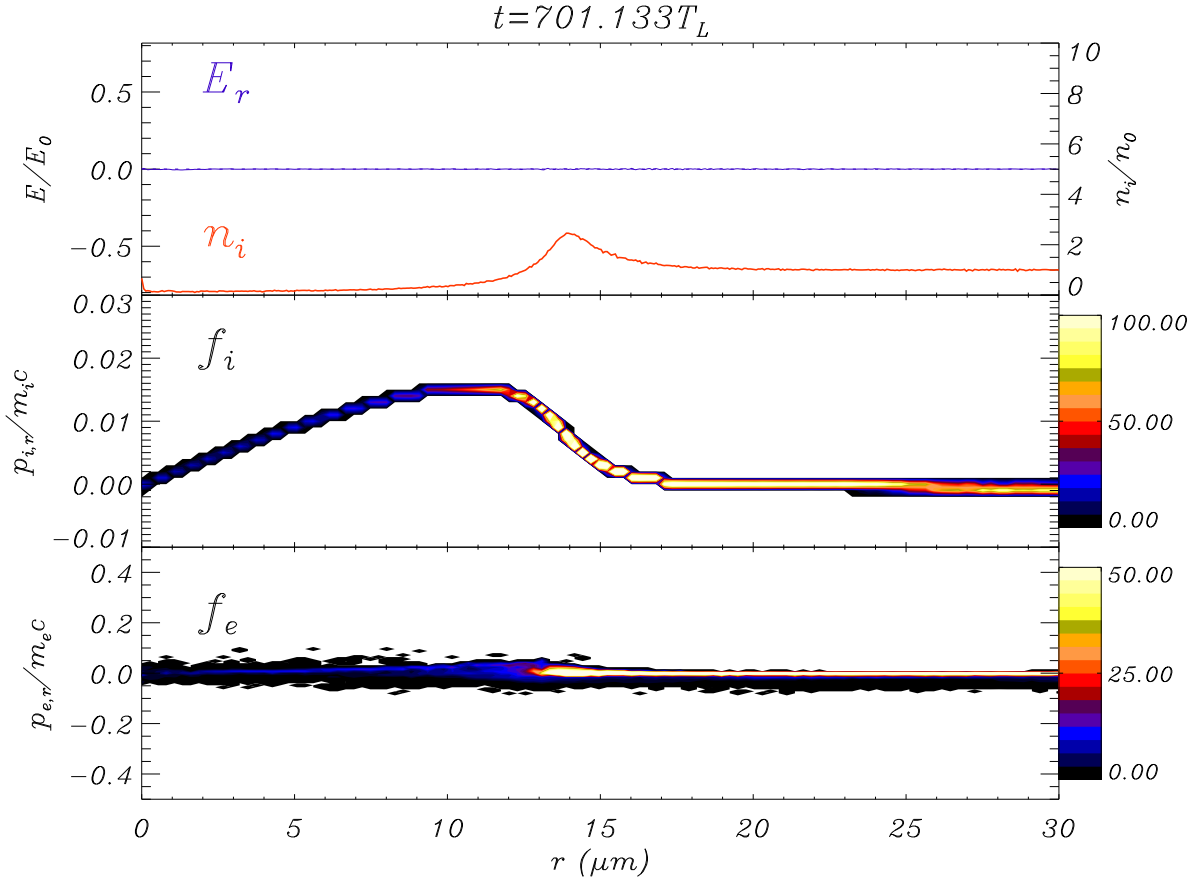

Echo effect is due to “breaking”

Analysis of ion phase space show that hydrodynamical breaking occurs when faster ions overlap the slowest ones

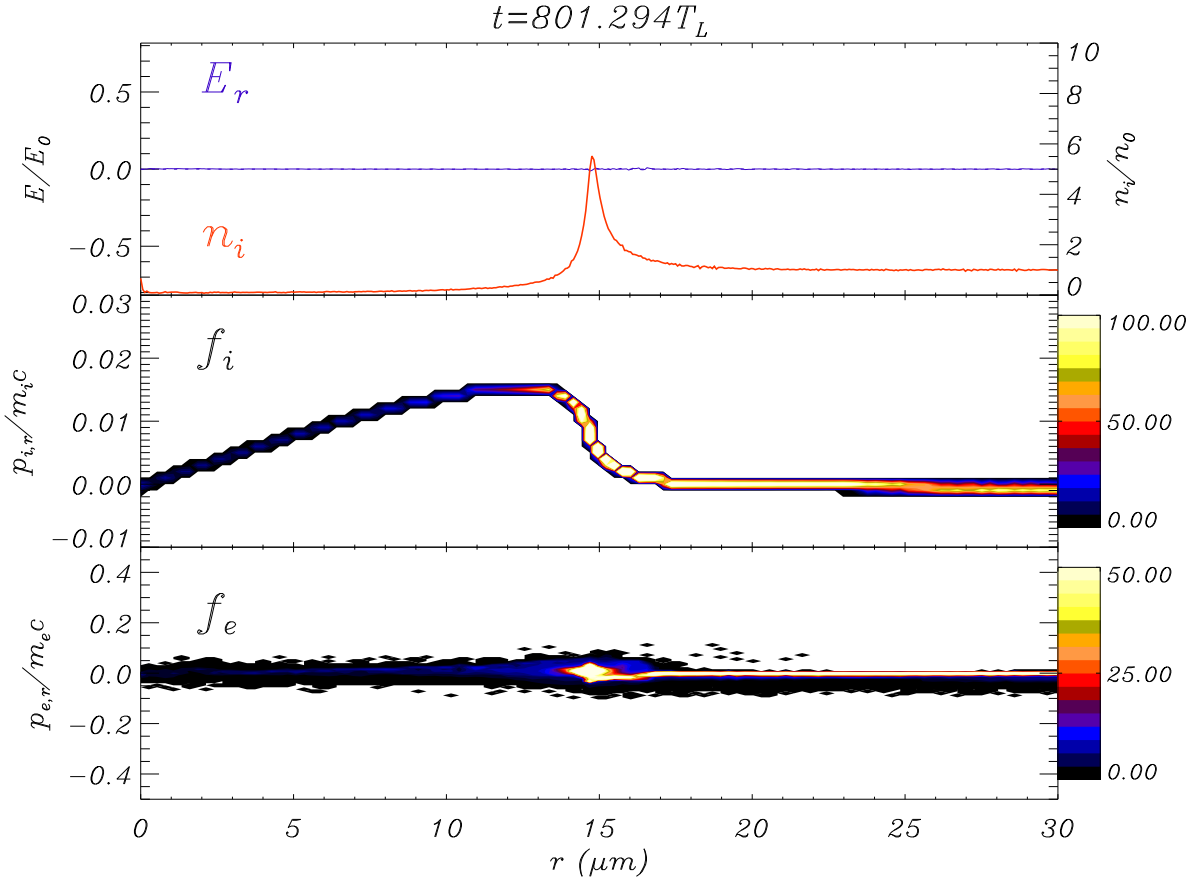

Echo effect is due to “breaking”

Analysis of ion phase space show that hydrodynamical breaking occurs when faster ions overlap the slowest ones

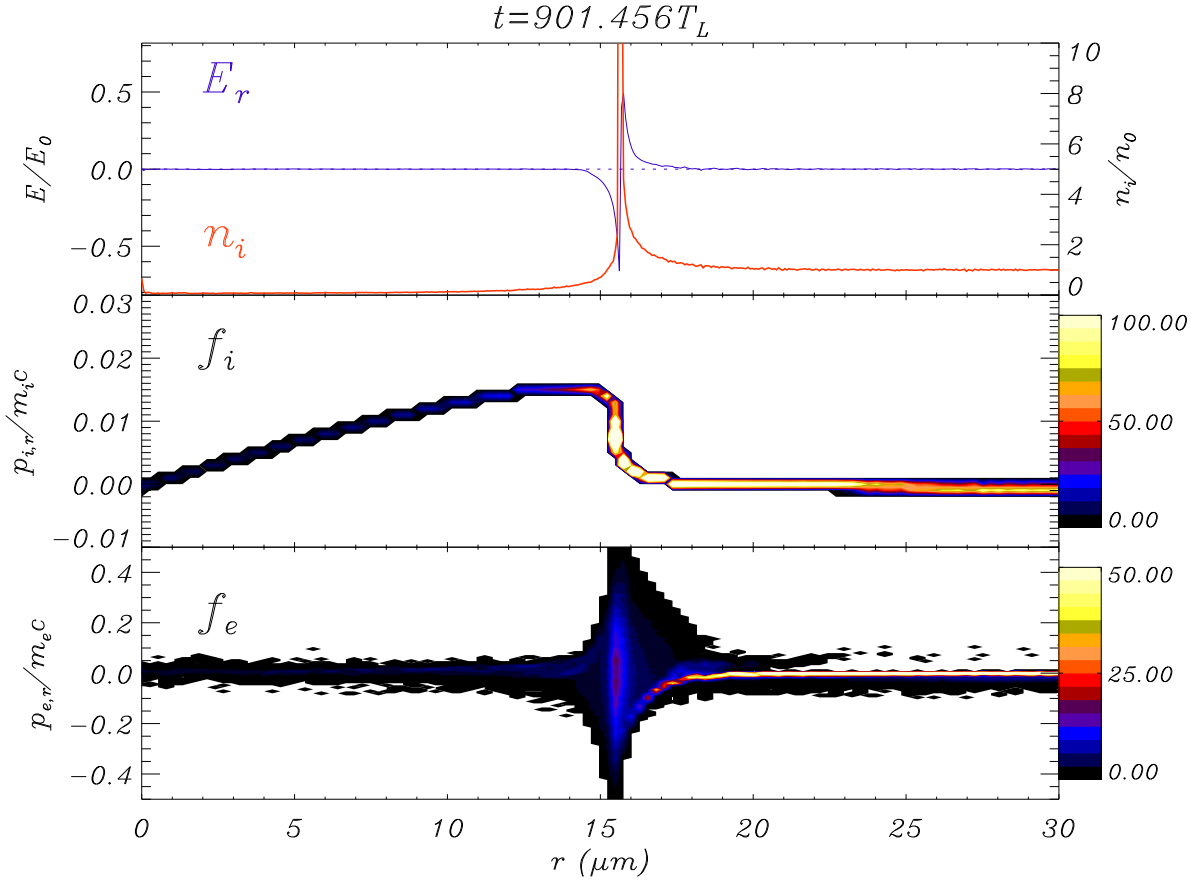

At breaking, strong electron heating occurs

A “sheath” ambipolar field is generated around the density spike

Echo effect is due to “breaking”

Analysis of ion phase space show that hydrodynamical breaking occurs when faster ions overlap the slowest ones

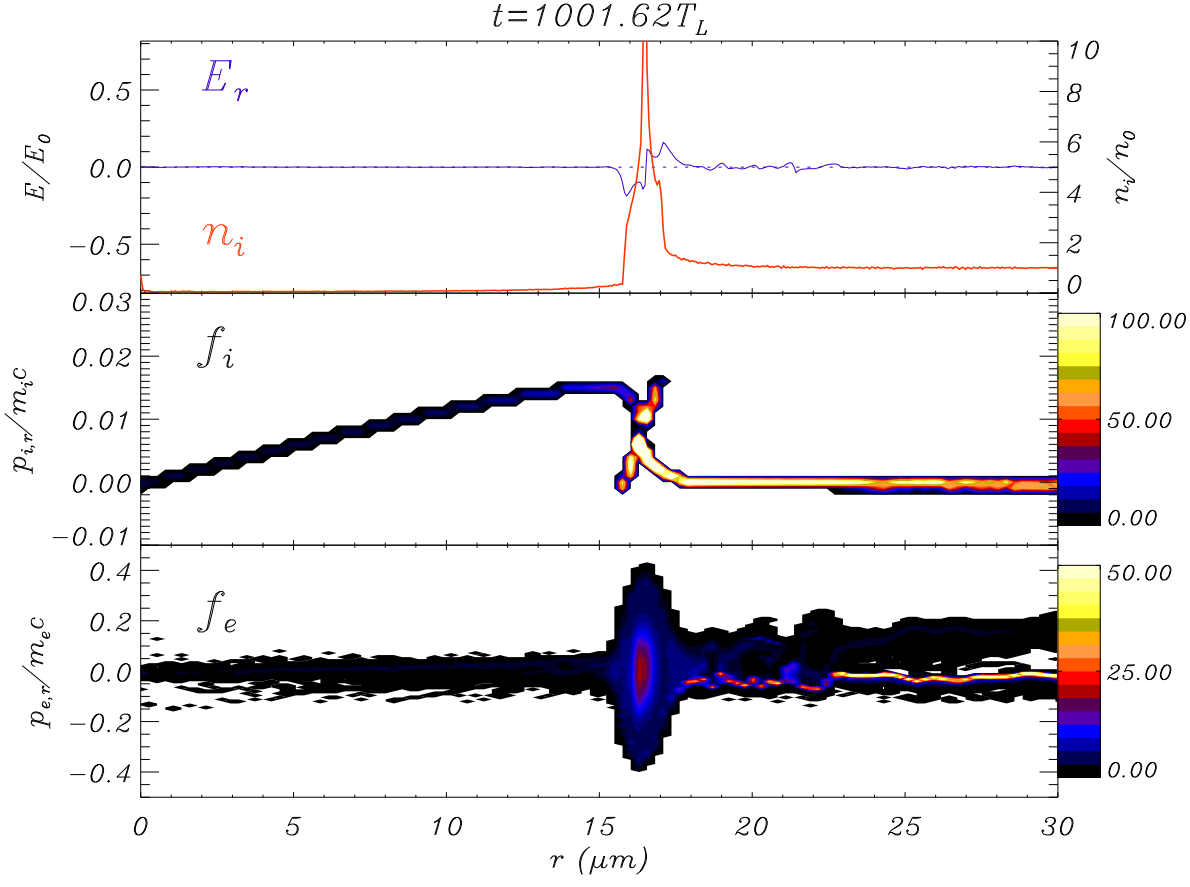

At breaking, strong electron heating occurs

A “sheath” ambipolar field is generated around the density spike

Echo effect is due to “breaking”

Analysis of ion phase space show that hydrodynamical breaking occurs when faster ions overlap the slowest ones

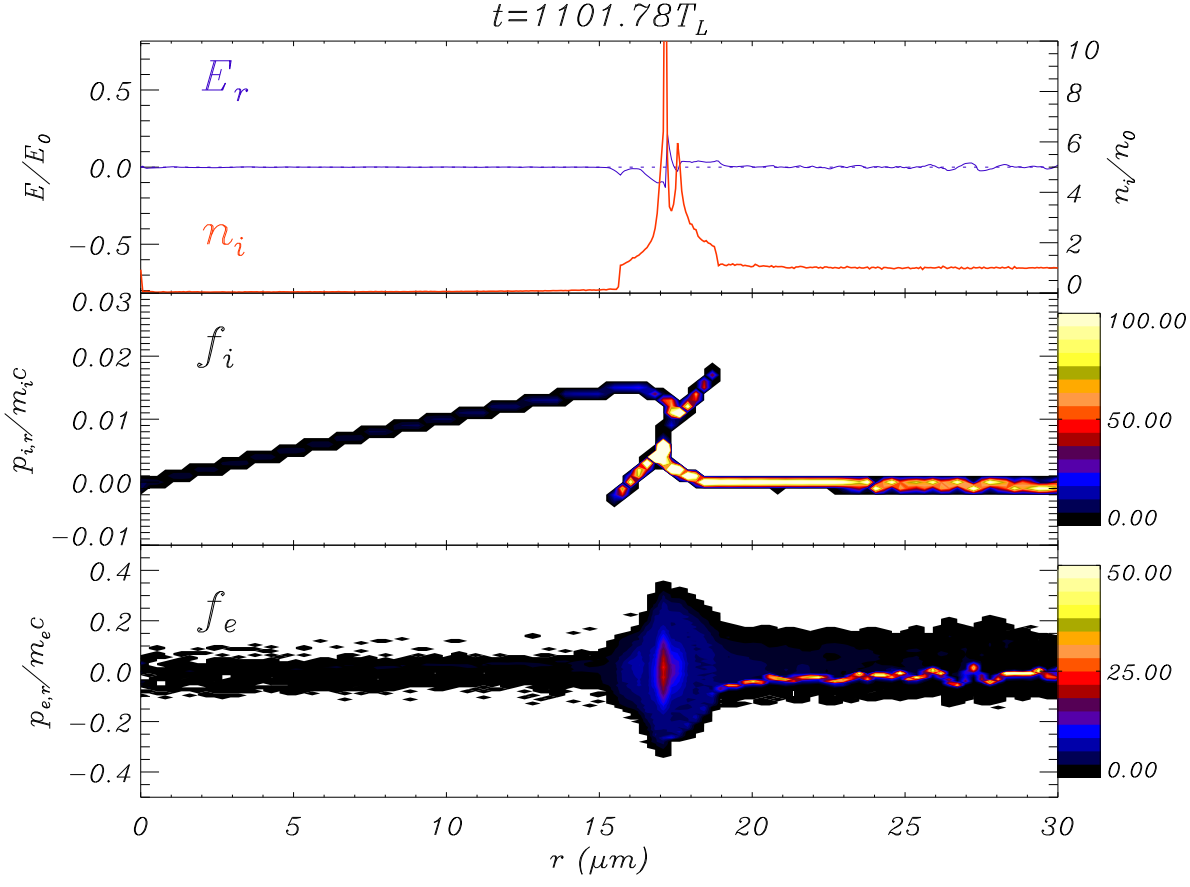

At breaking, strong electron heating occurs

A “sheath” ambipolar field is generated around the density spike

Echo effect is due to “breaking”

Analysis of ion phase space show that hydrodynamical breaking occurs when faster ions overlap the slowest ones

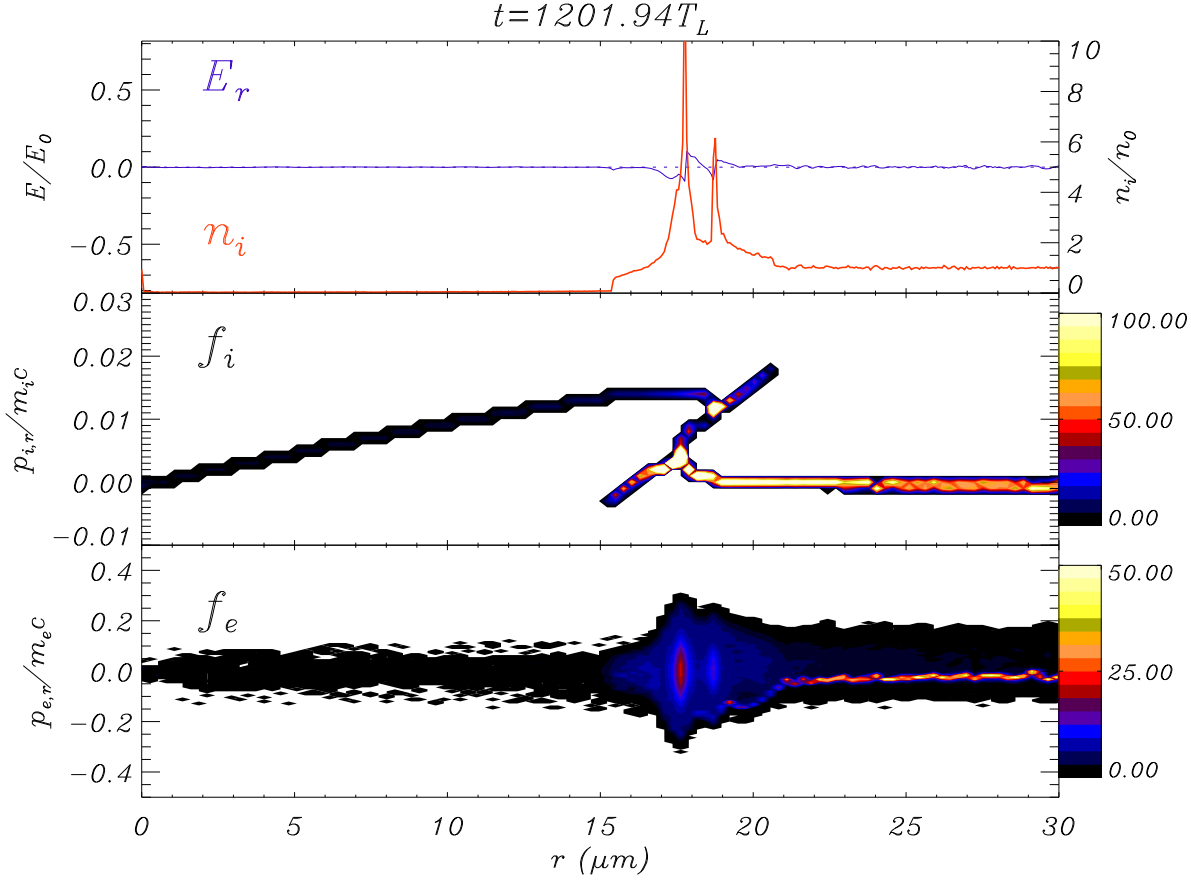

At breaking, strong electron heating occurs

A “sheath” ambipolar field is generated around the density spike

Echo effect is due to “breaking”

Analysis of ion phase space show that hydrodynamical breaking occurs when faster ions overlap the slowest ones

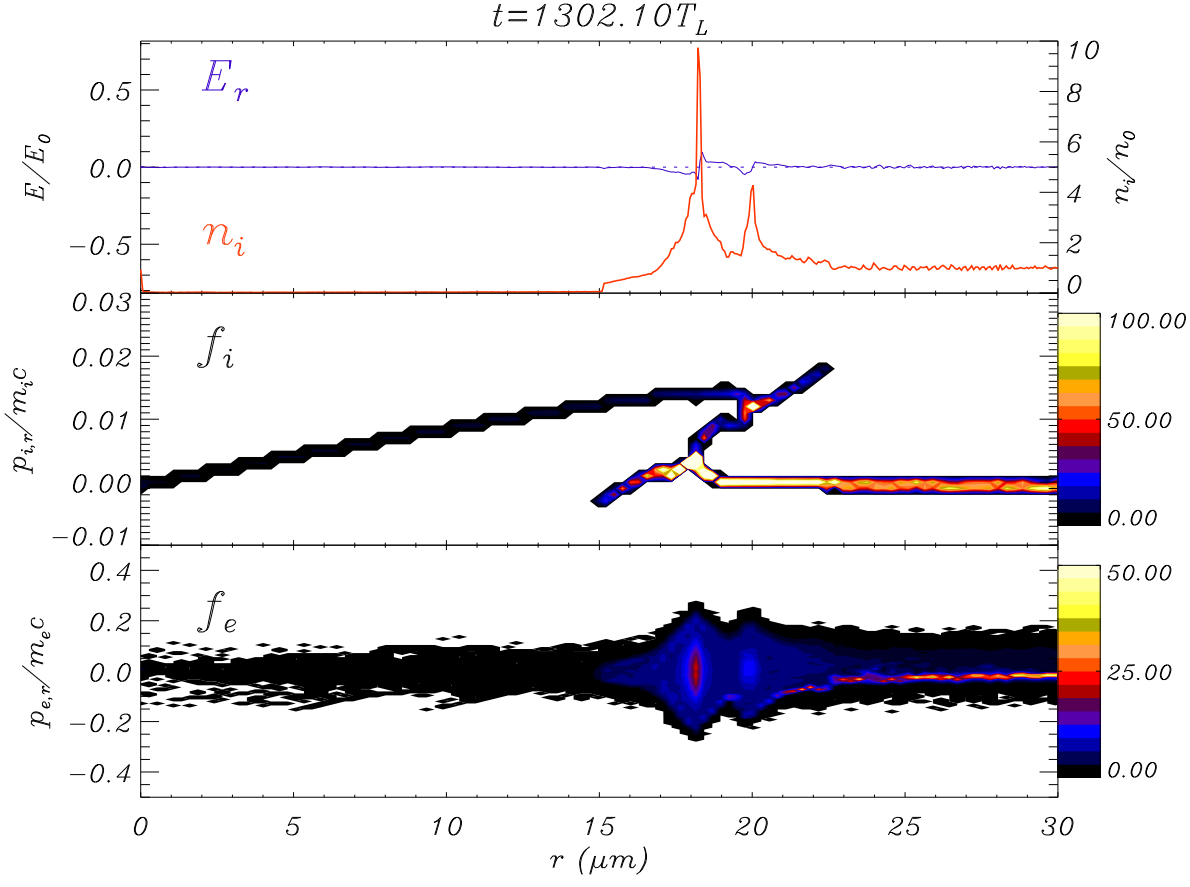

At breaking, strong electron heating occurs

A “sheath” ambipolar field is generated around the density spike

Beam breakup

Beam breakup

The laser pulse breaks into three “filaments” originating near the location of the ion density breaking

Beam breakup

The laser pulse breaks into three “filaments” originating near the location of the ion density breaking

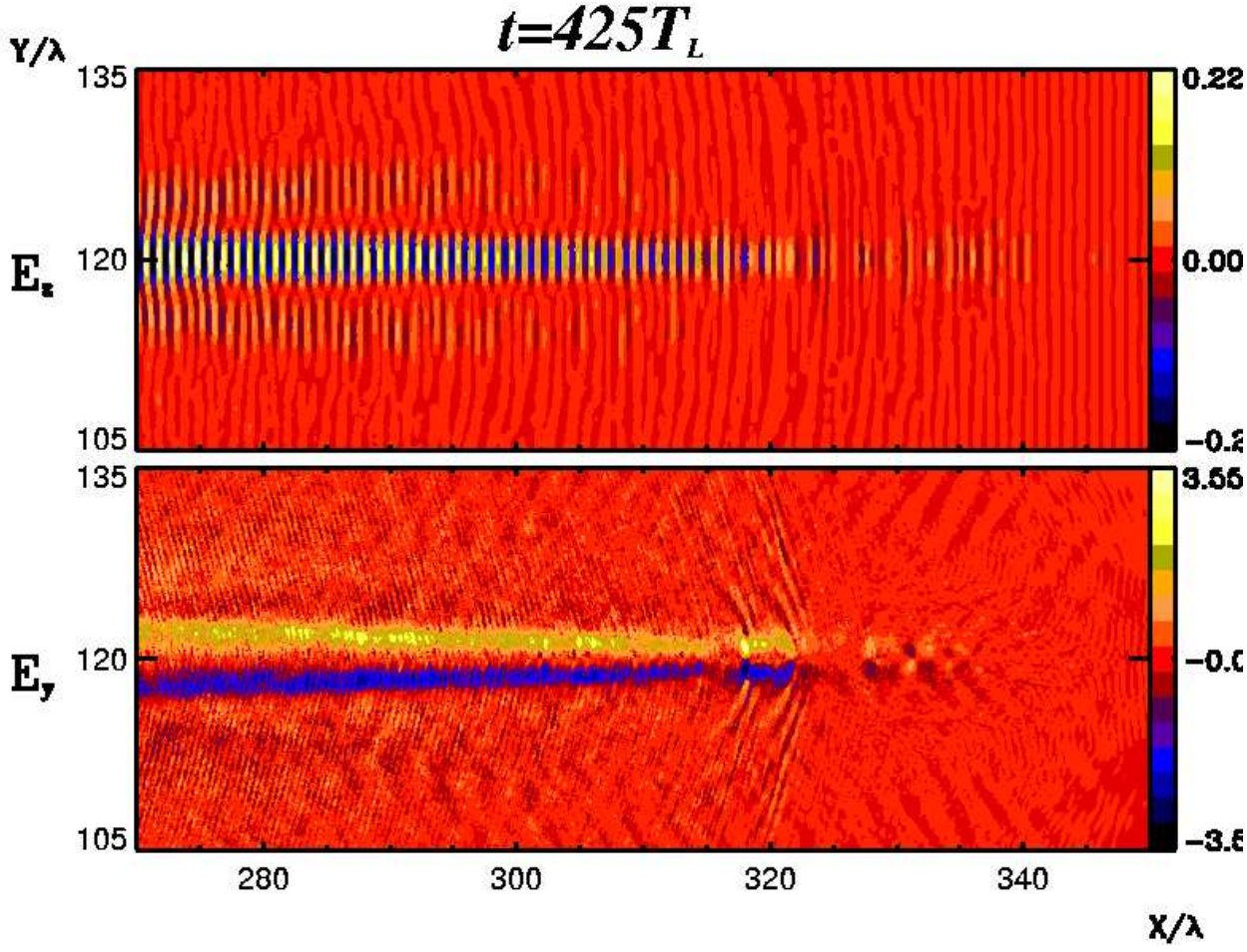

Beam breakup

The laser pulse breaks into three “filaments” originating near the location of the ion density breaking

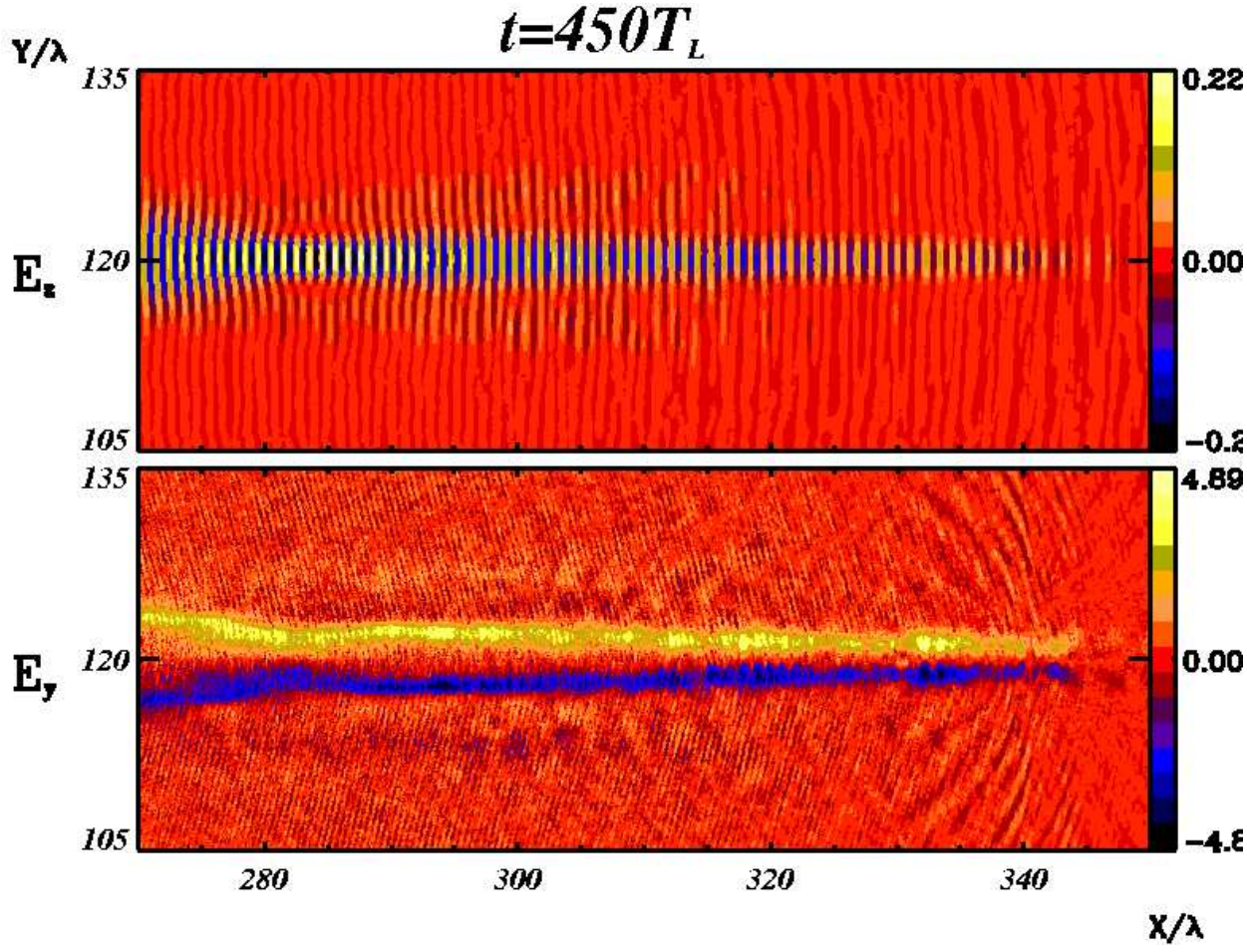

Beam breakup

The laser pulse breaks into three “filaments” originating near the location of the ion density breaking

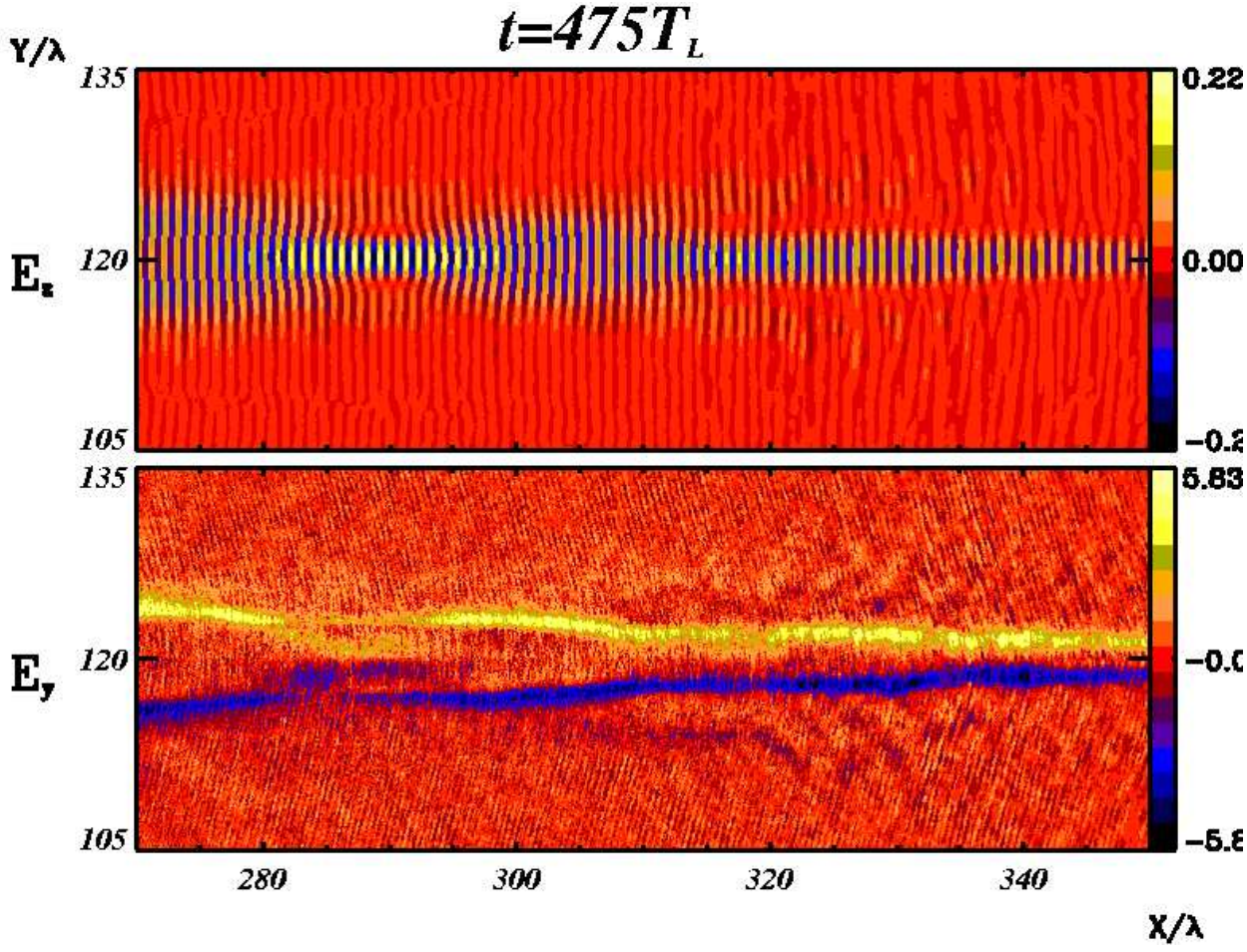

Beam breakup

The laser pulse breaks into three “filaments” originating near the location of the ion density breaking

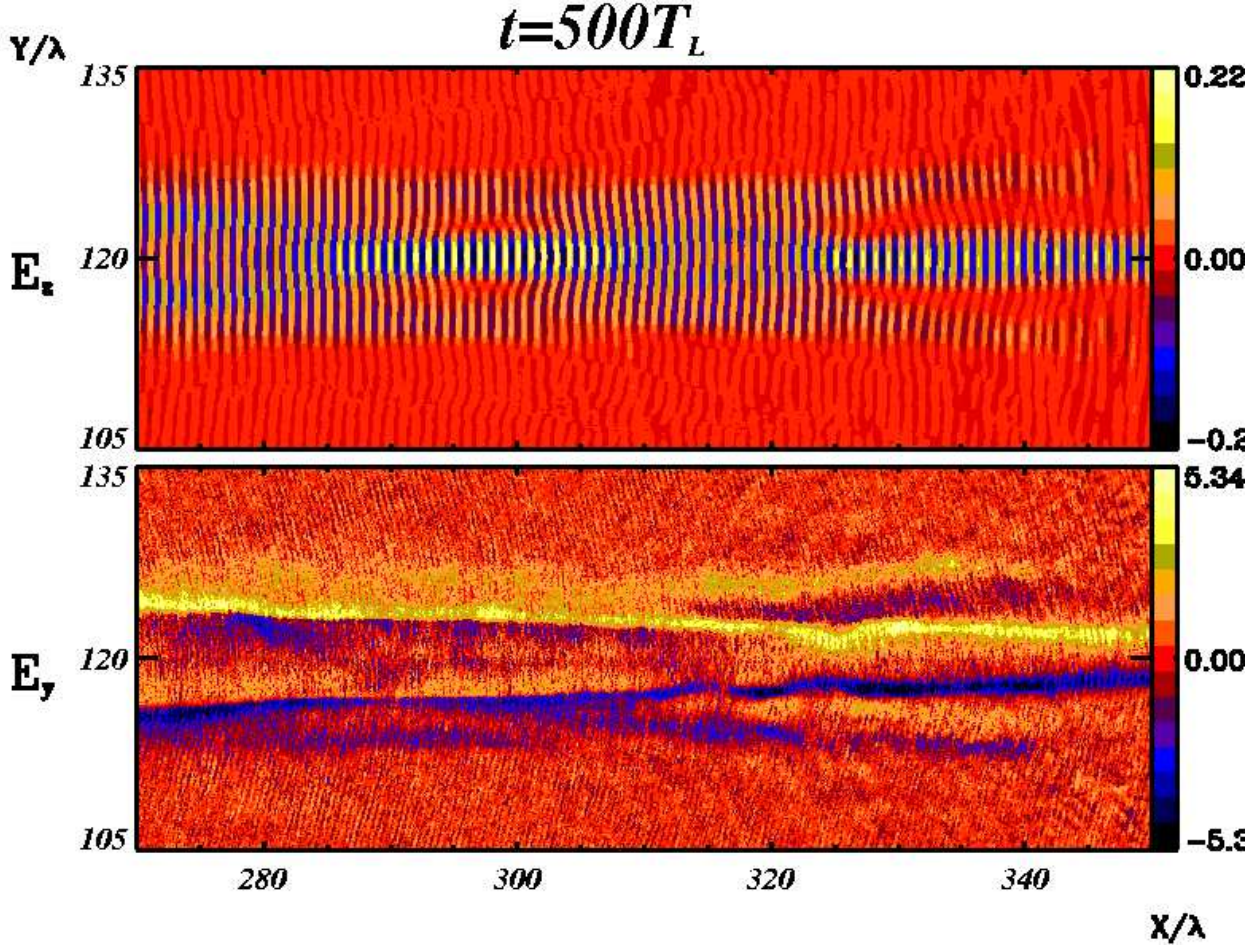

Beam breakup

The laser pulse breaks into three “filaments” originating near the location of the ion density breaking

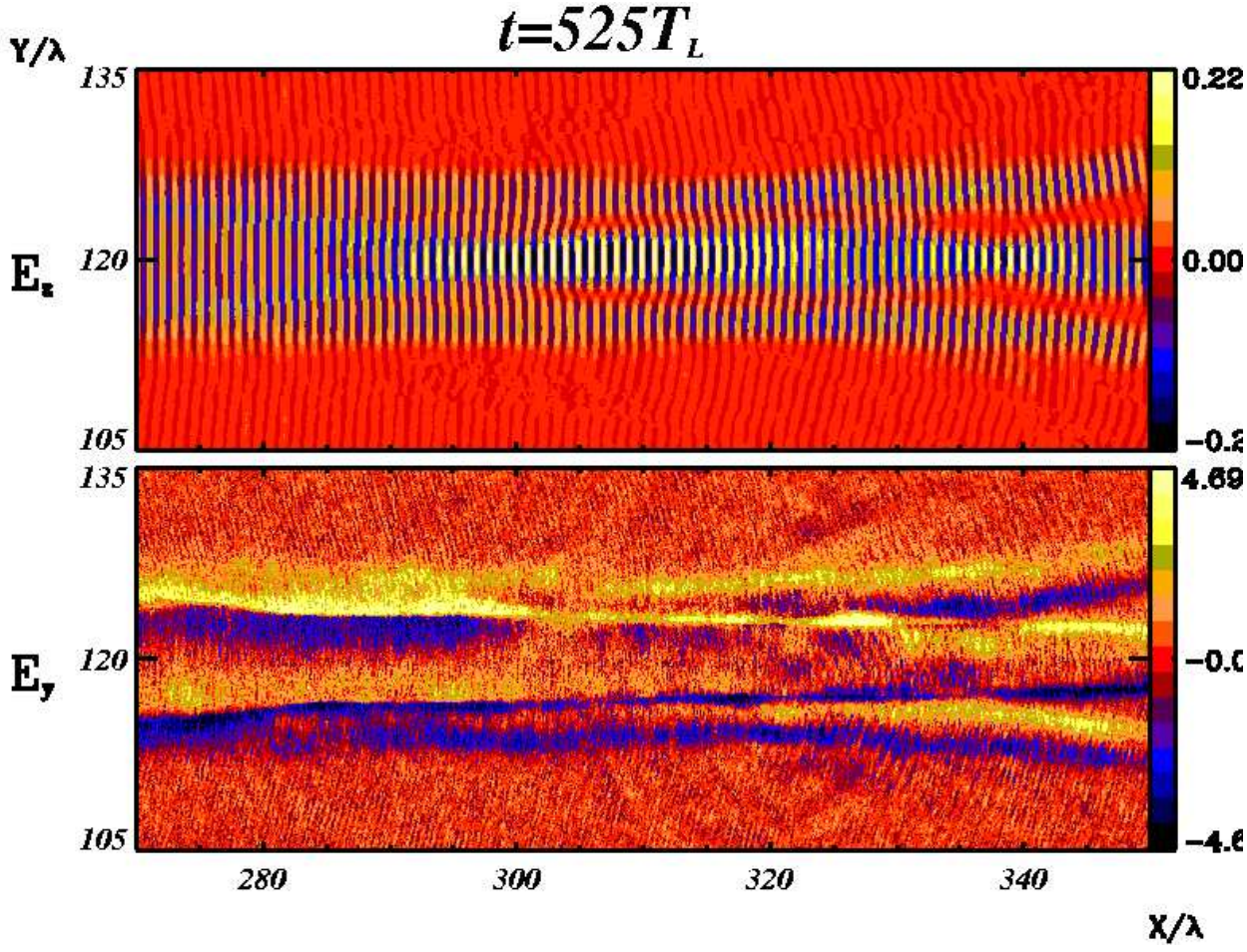

Beam breakup

The laser pulse breaks into three “filaments” originating near the location of the ion density breaking

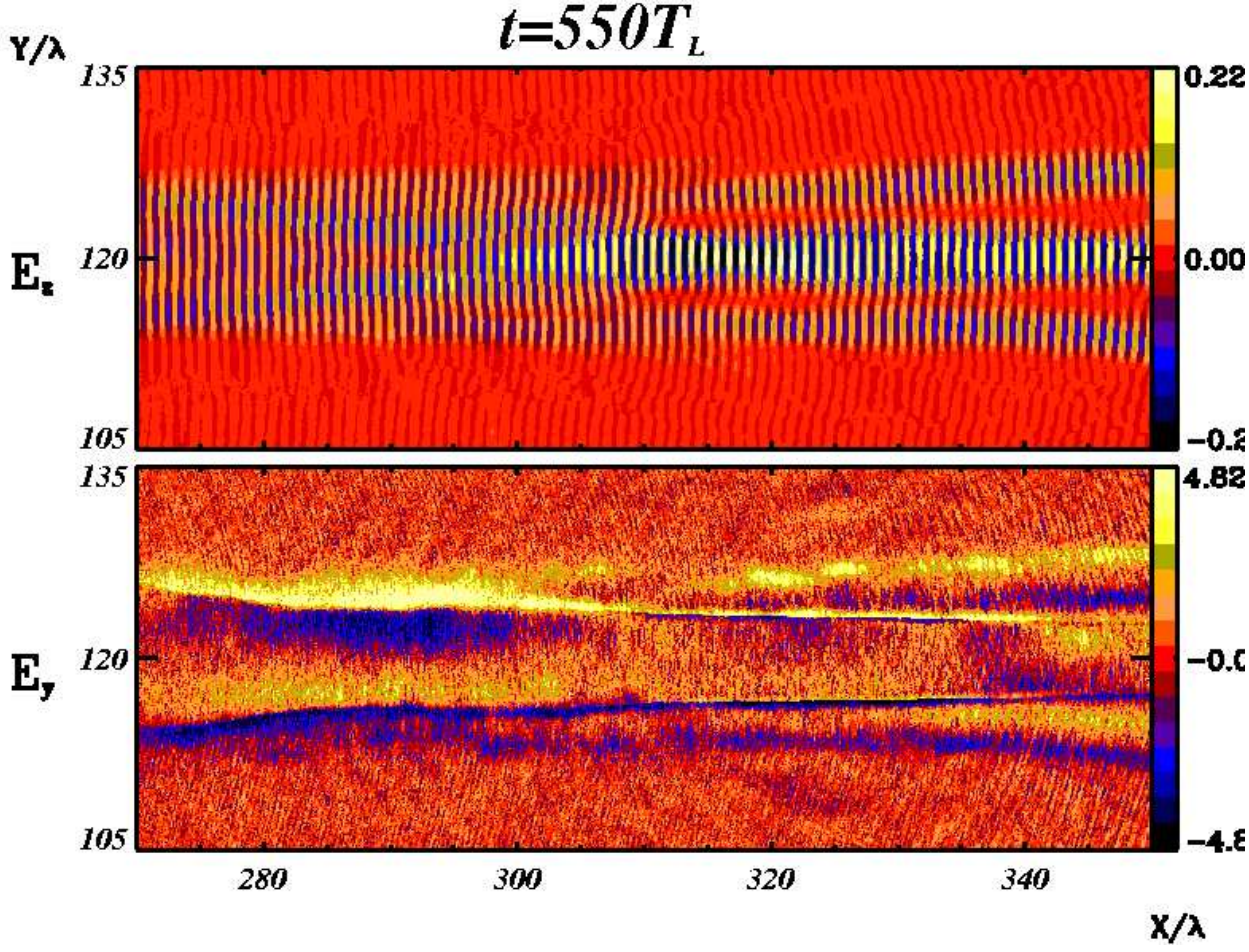

Beam breakup

The laser pulse breaks into three “filaments” originating near the location of the ion density breaking

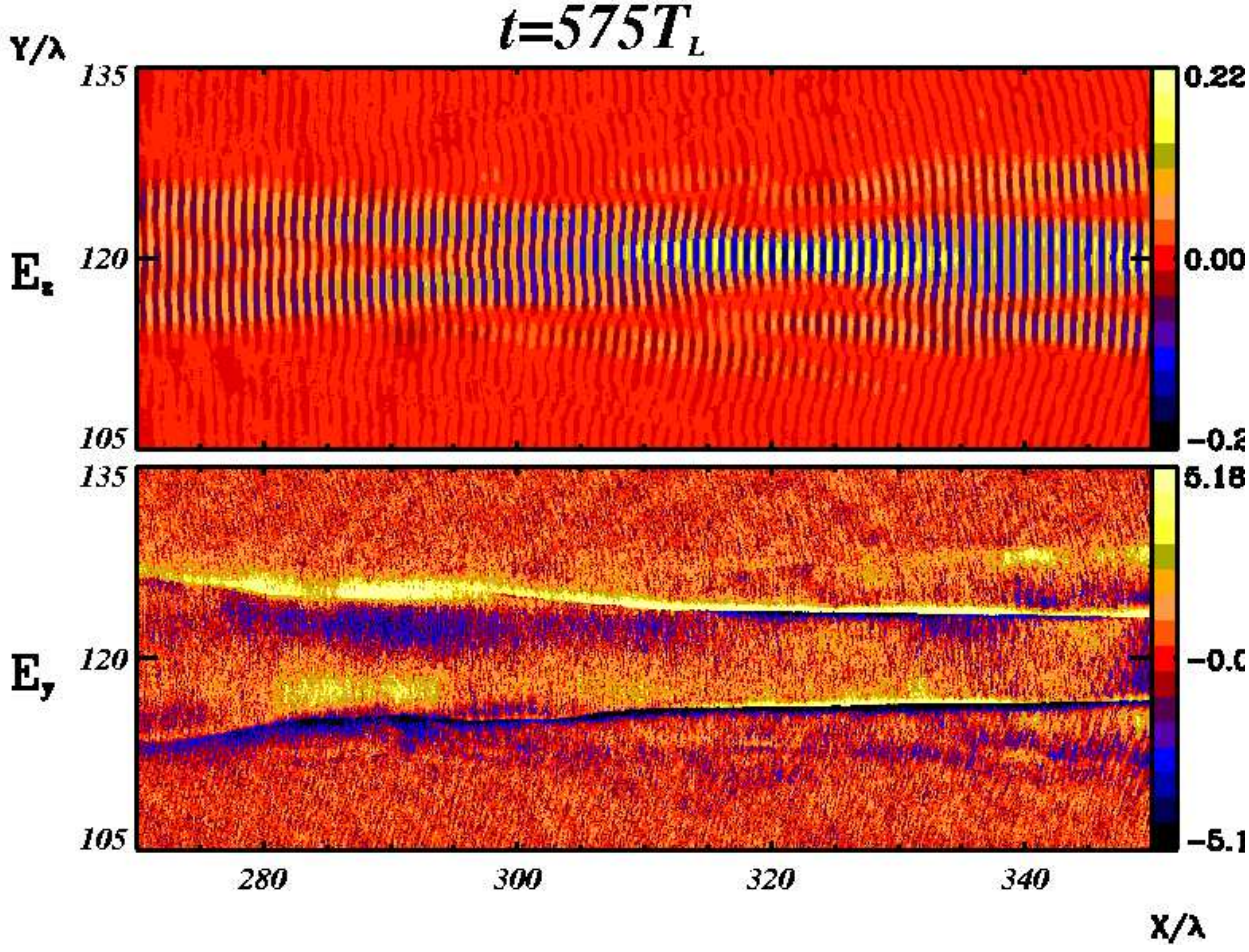

Beam breakup

The laser pulse breaks into three “filaments” originating near the location of the ion density breaking

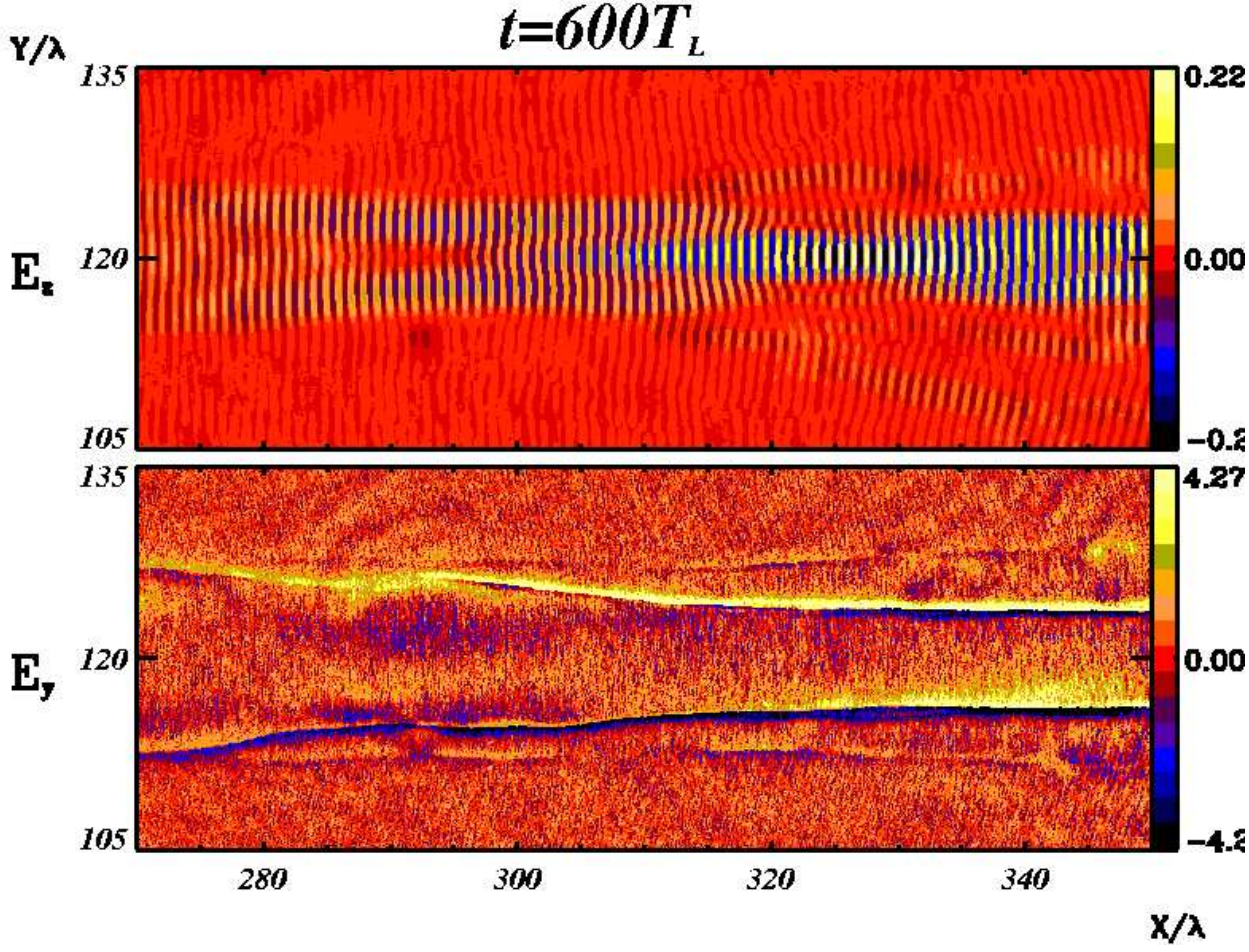

Beam breakup

The laser pulse breaks into three “filaments” originating near the location of the ion density breaking

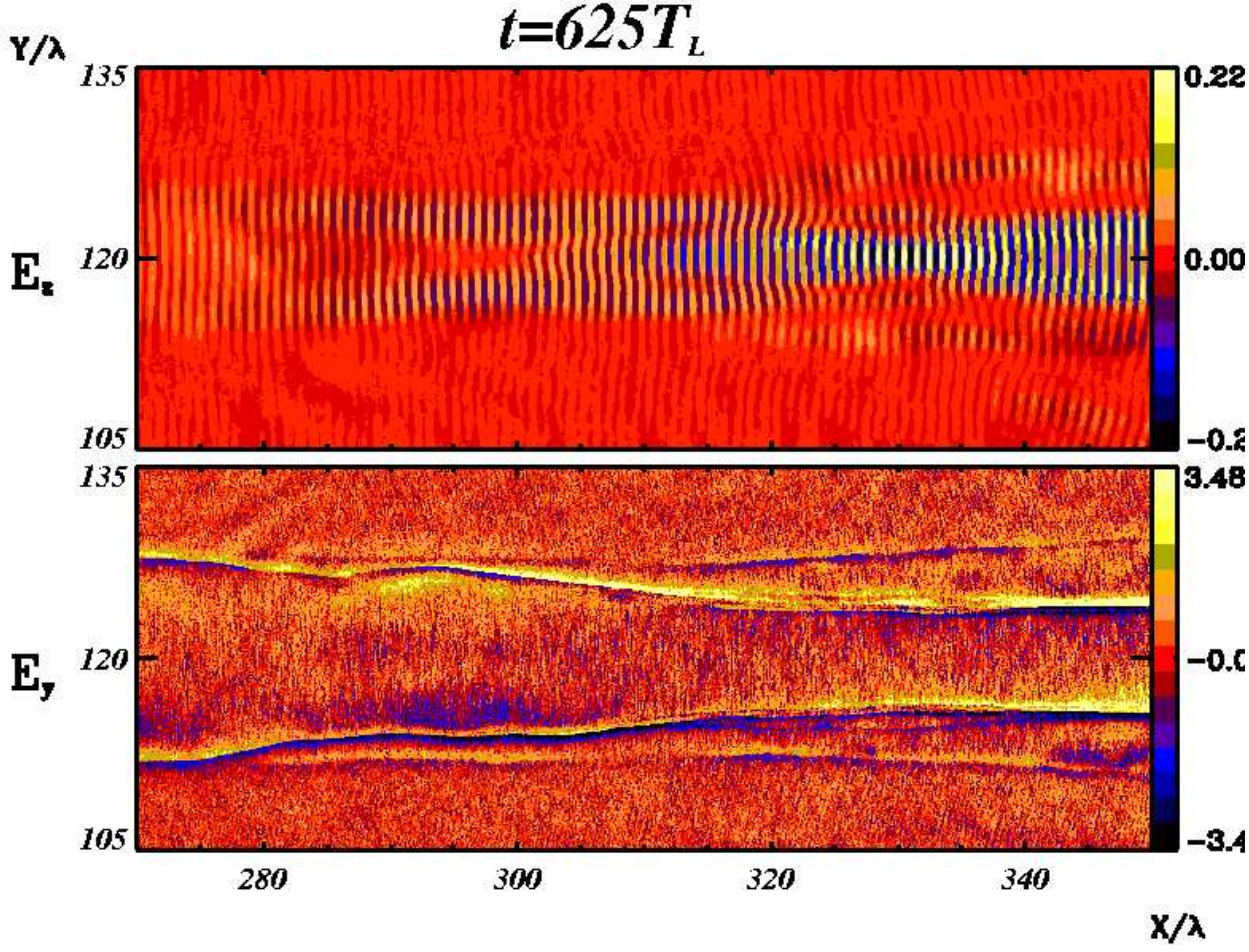

Beam breakup

The laser pulse breaks into three “filaments” originating near the location of the ion density breaking

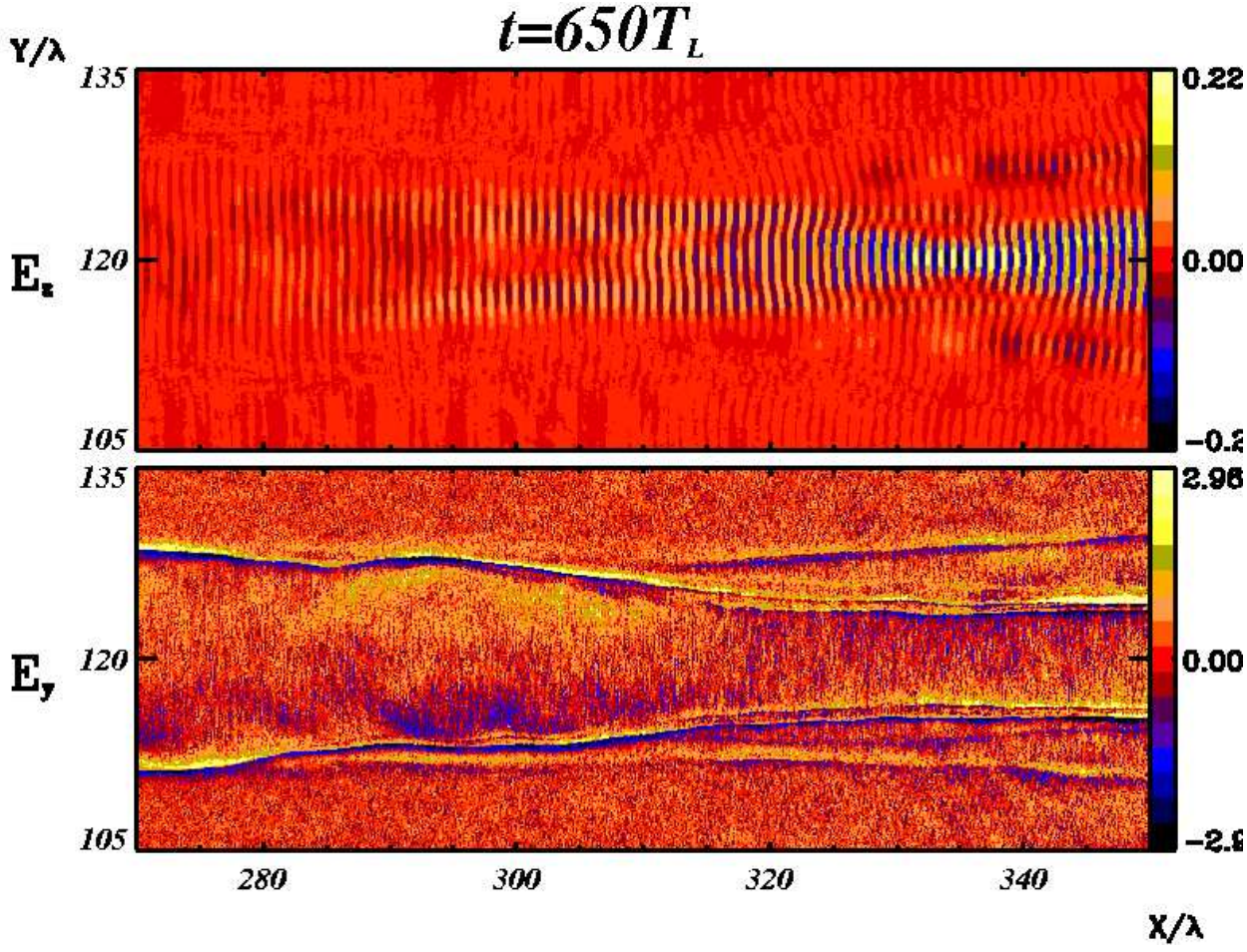

Leaking waveguide model

Leaking waveguide model

The self-guided laser pulse can be roughly modeled by two overlapping plane waves with $\mathbf{k}_1 = (k_x, k_y)$, $\mathbf{k}_2 = (k_x, -k_y)$,

$$k_y = \frac{\pi}{d}, k_x = \sqrt{\frac{\omega^2}{c^2} - k_y^2}$$

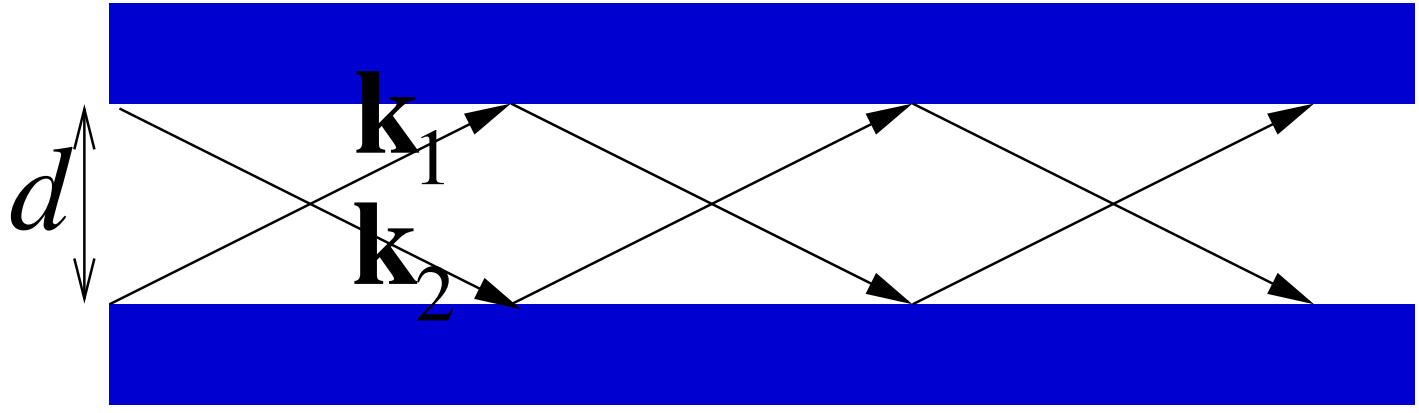

Leaking waveguide model

A sudden “leak” in the channel walls leads to the escape of radiation at an angle

$$\theta \simeq \arctan\left(\frac{k_y}{k_x}\right)$$

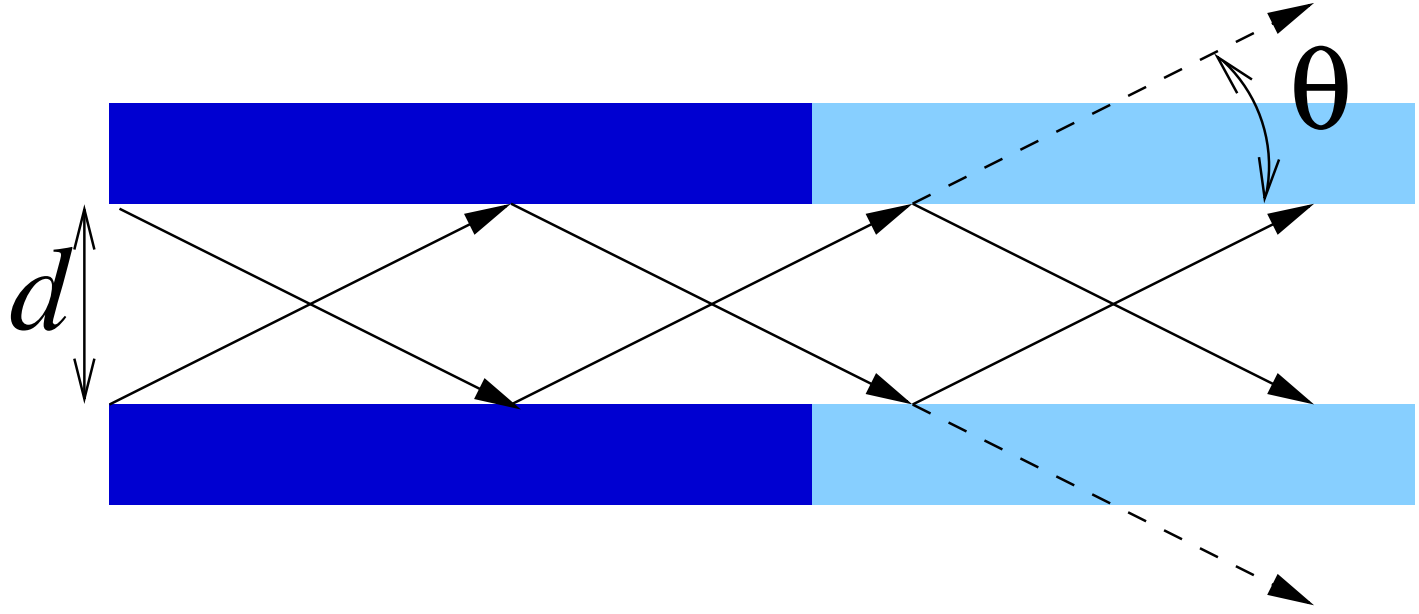

Leaking waveguide model

From the simulation $d \simeq 7\lambda$ near the breaking point

$$\tan\theta \simeq 0.065, \qquad \frac{k_y}{k_x} \simeq \frac{\lambda}{2d} \simeq \frac{1}{14} = 0.071$$

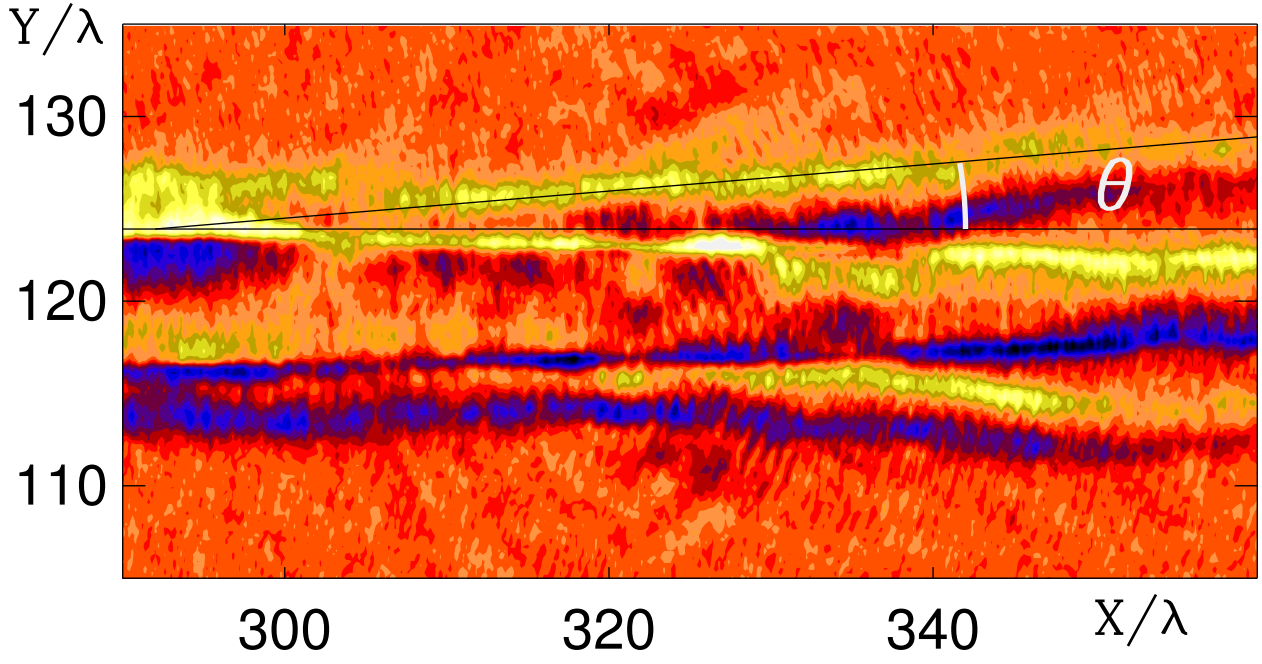

Slowly-varying structures

Slowly-varying structures

Generation of both isolated and pattern-organized field structures

Slowly-varying structures

Generation of both isolated and pattern-organized field structures

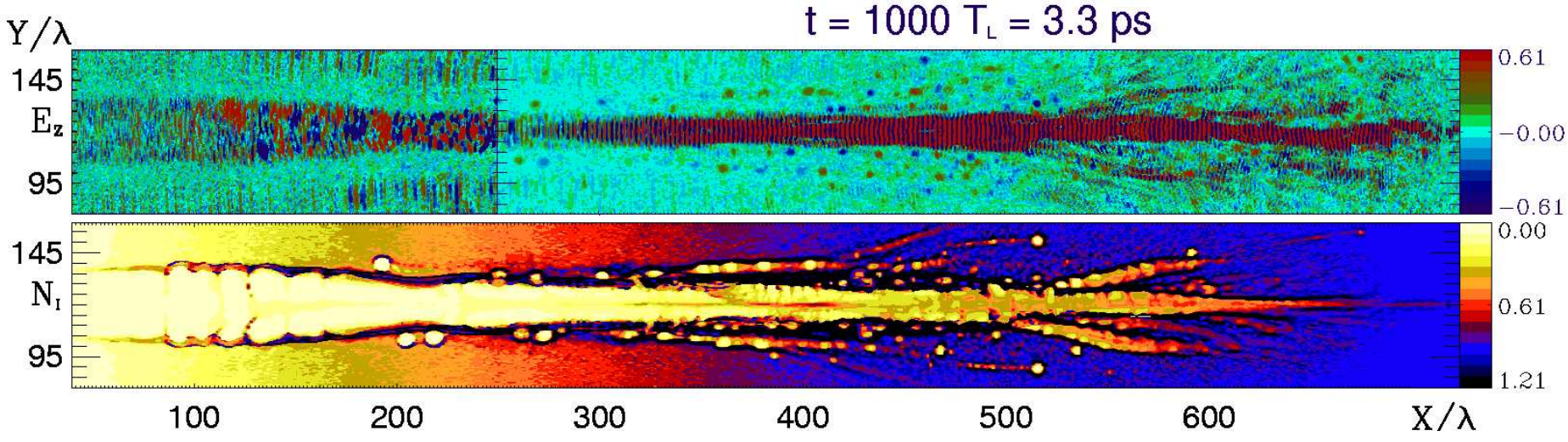

Slowly-varying structures

Both isolated “cavitons” or “post-solitons” and patterns inside density channels

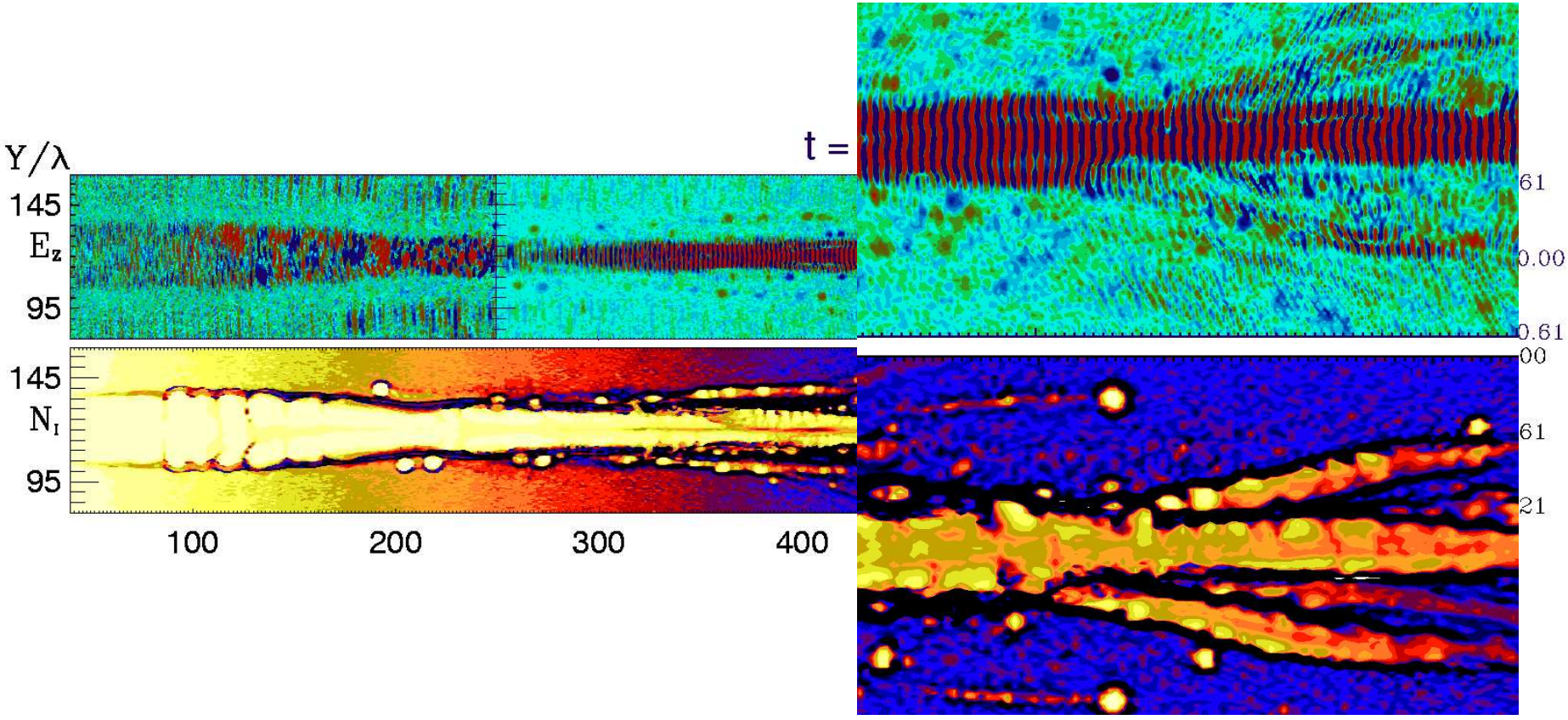

Slowly-varying structures

Axially symmetrical pattern inside the main channel, in the low-density region

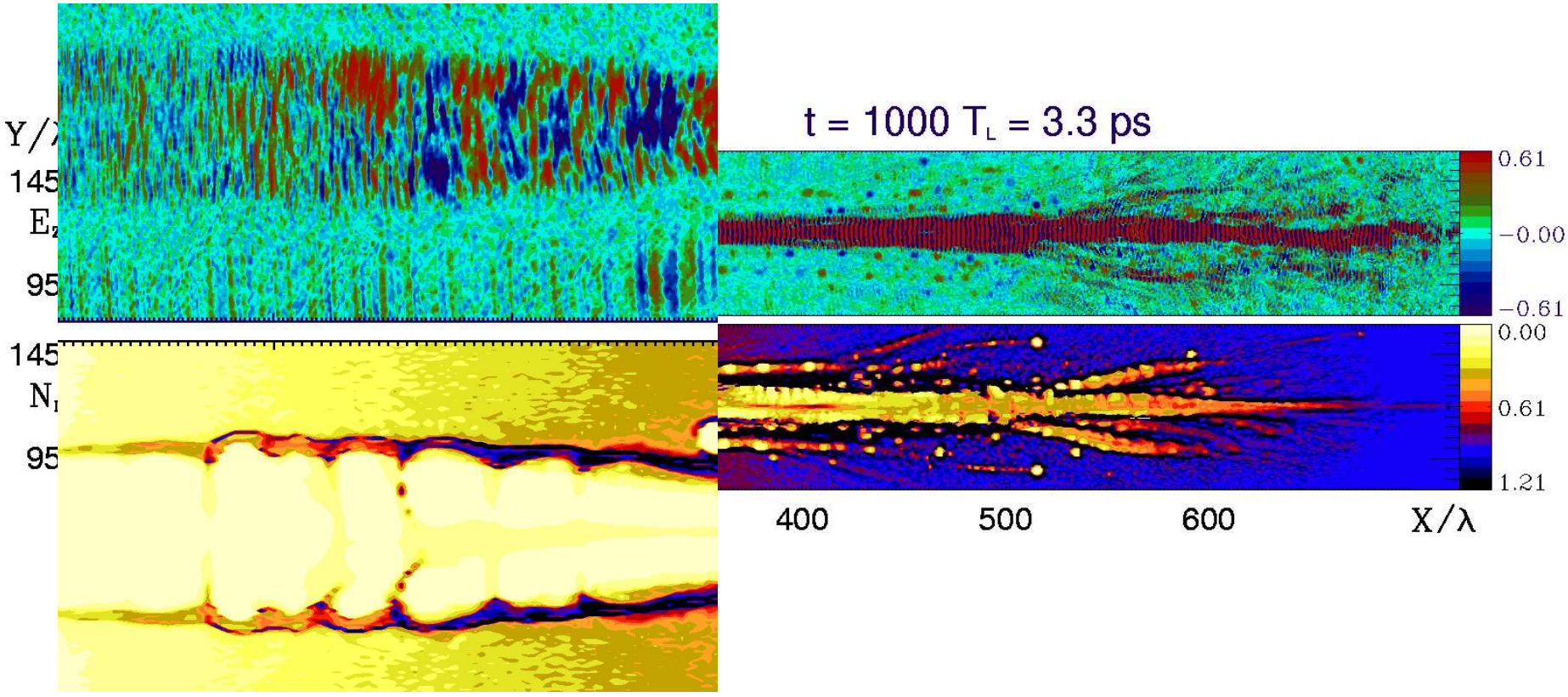

Evolution of field structures

Evolution of field structures

Pattern of standing “cavitons” grow inside low-density channels (due to the trapping of low-frequency light?)

Evolution of field structures

Pattern of standing “cavitons” grow inside low-density channels (due to the trapping of low-frequency light?)

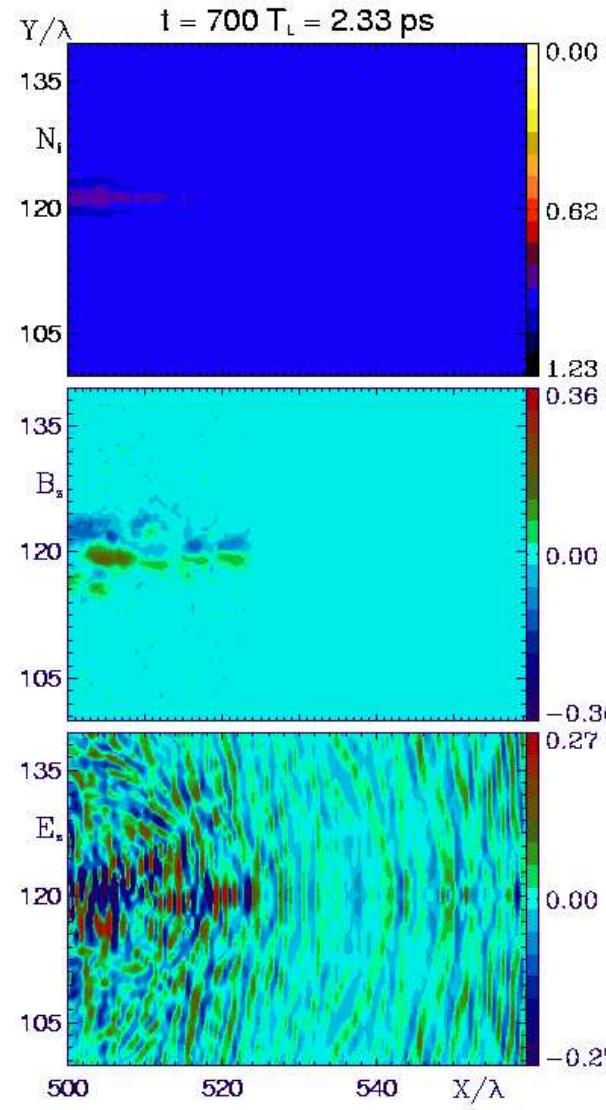

Evolution of field structures

Pattern of standing “cavitons” grow inside low-density channels (due to the trapping of low-frequency light?)

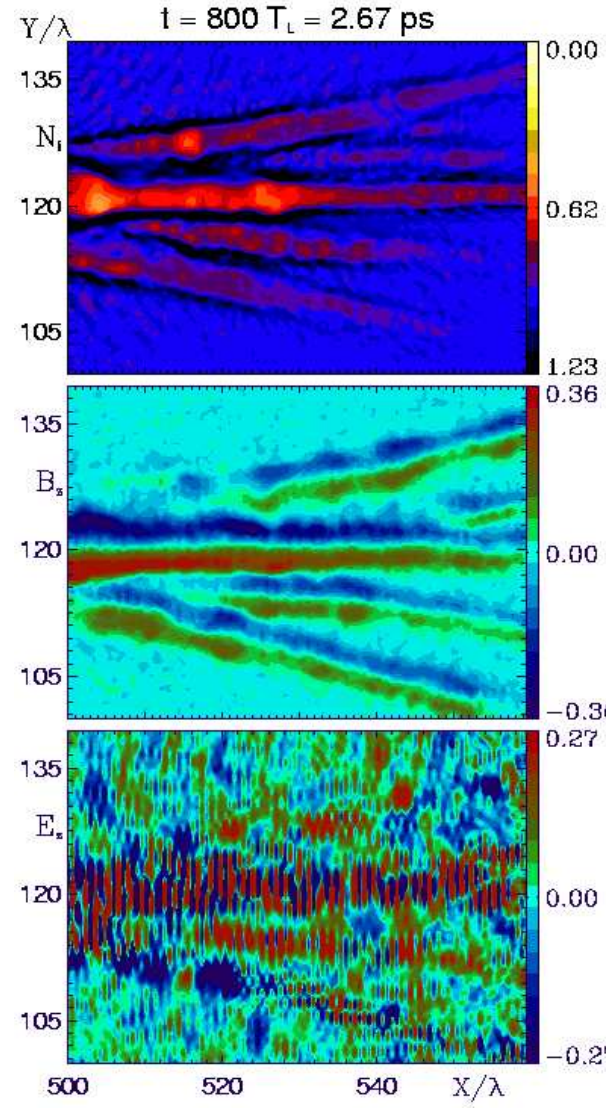

Evolution of field structures

Pattern of standing “cavitons” grow inside low-density channels (due to the trapping of low-frequency light?)

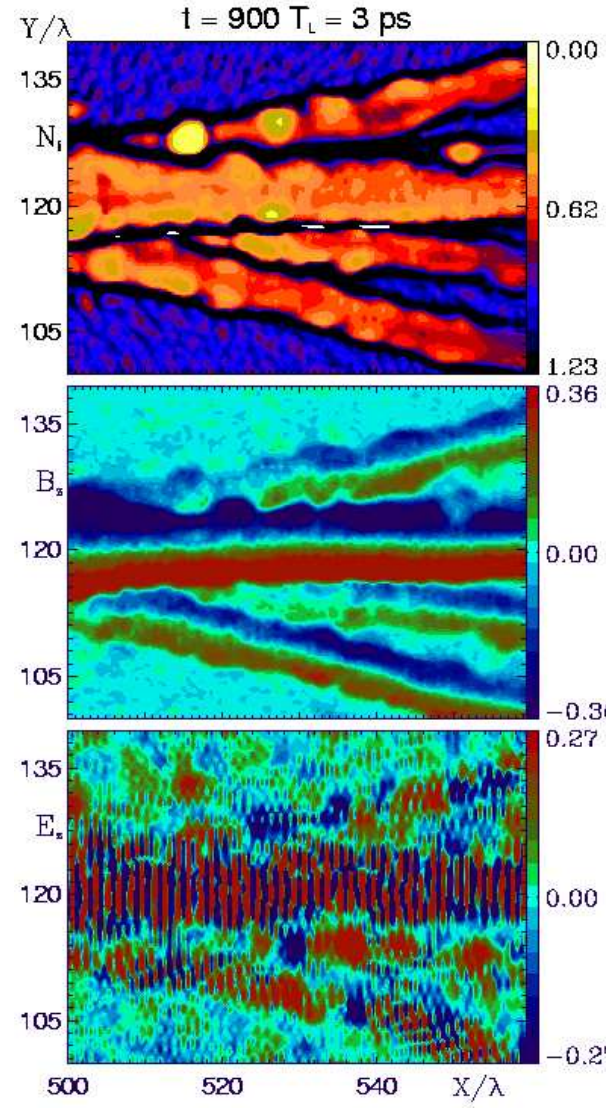

Evolution of field structures

Pattern of standing “cavitons” grow inside low-density channels (due to the trapping of low-frequency light?)

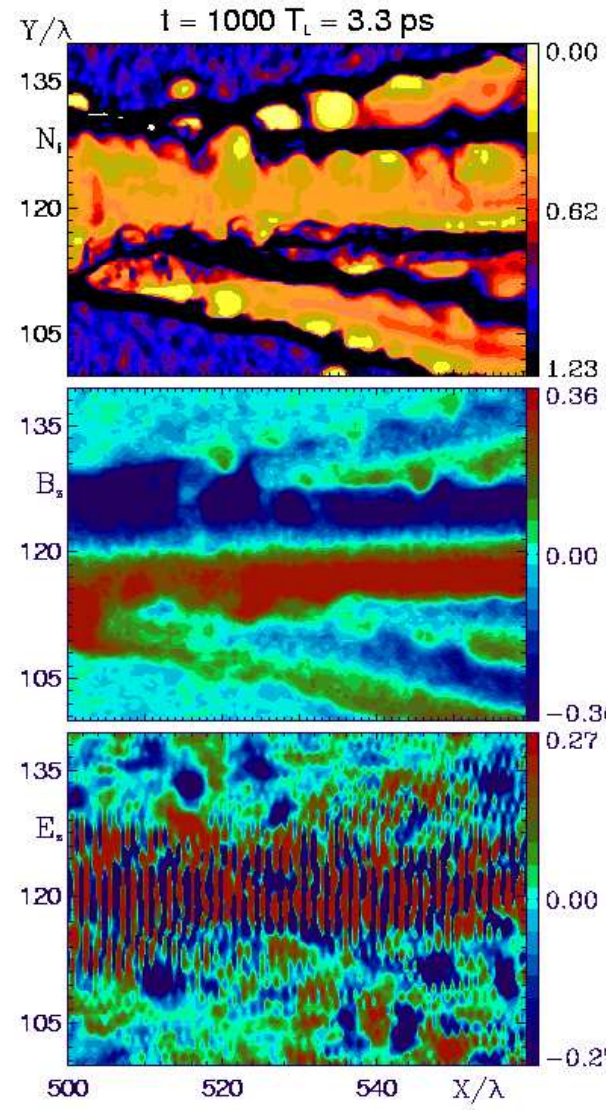

Evolution of field structures

Pattern of standing “cavitons” grow inside low-density channels (due to the trapping of low-frequency light?)

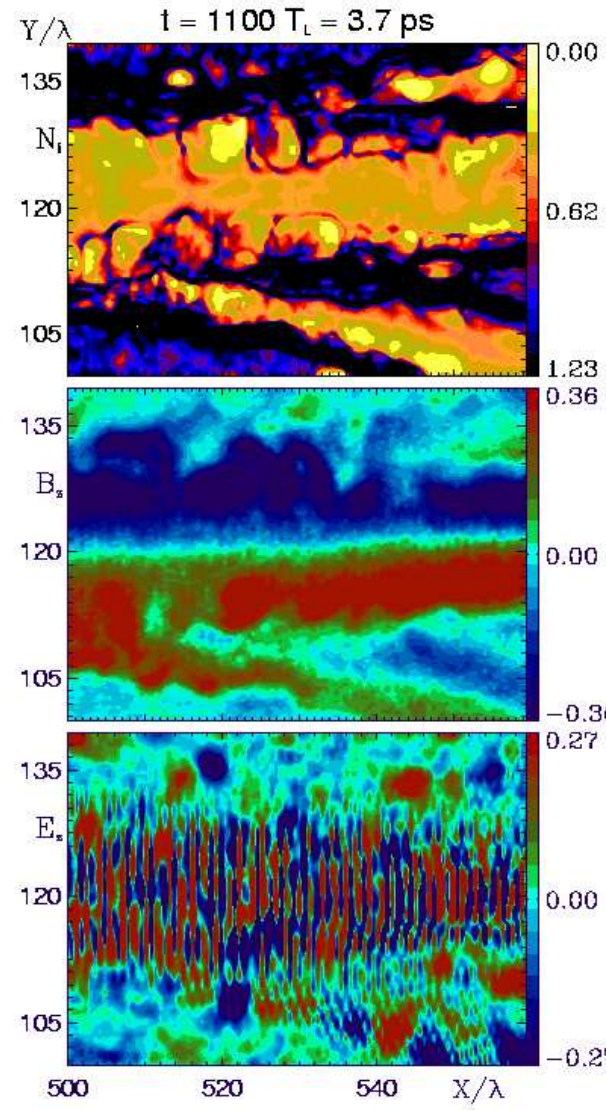

Evolution of field structures

Pattern of standing “cavitons” grow inside low-density channels (due to the trapping of low-frequency light?)

The are experimental indications of the growth of slowly varying field patterns inside channels

[see e.g. T.V.Liseikina et al, arXiv:physics/0702177]

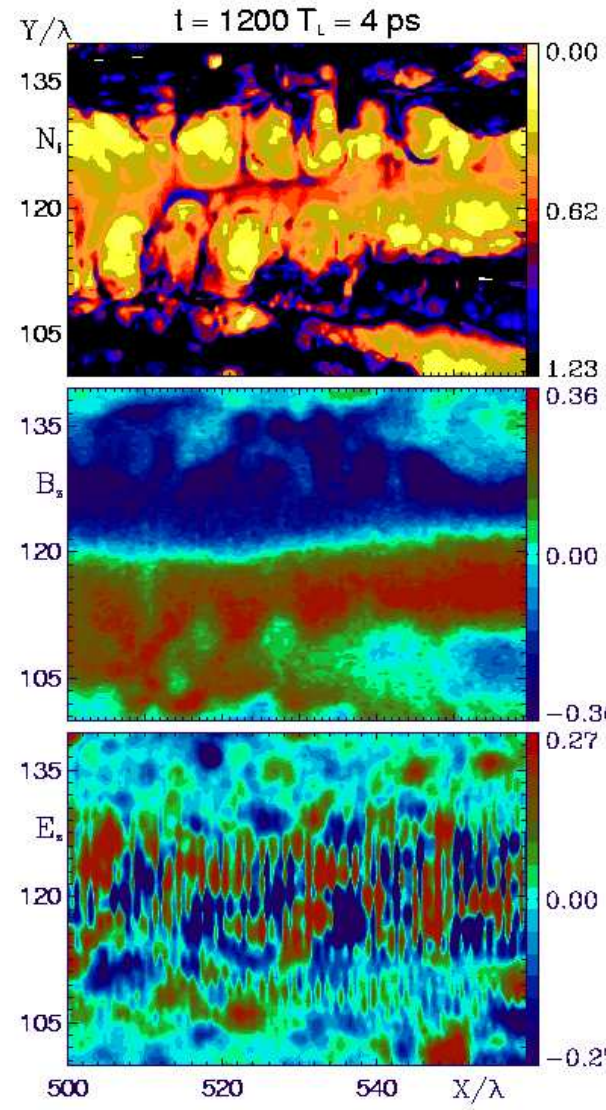

Hybrid structures

Hybrid structures

Structures from the pattern in the low-density region reveal a “hybrid” vortex-soliton nature with both oscillating and quasi-static components

Hybrid structures

Structures from the pattern in the low-density region reveal a “hybrid” vortex-soliton nature with both oscillating and quasi-static components

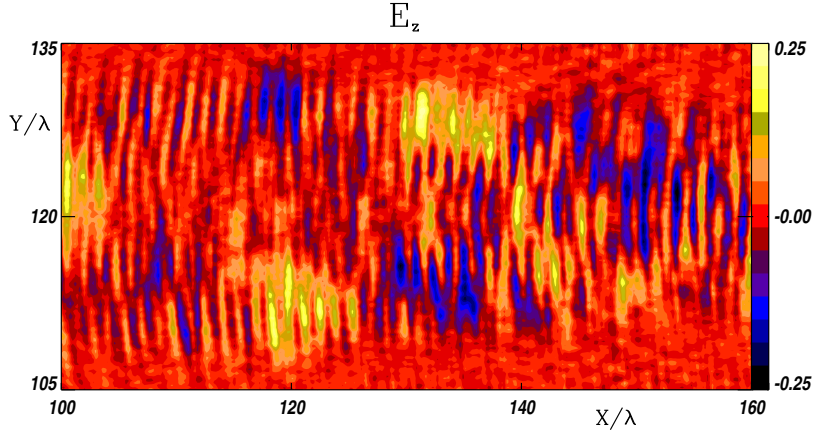

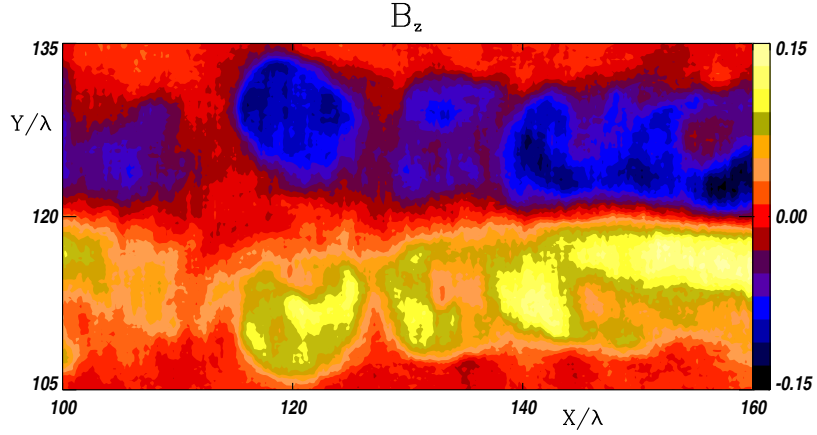

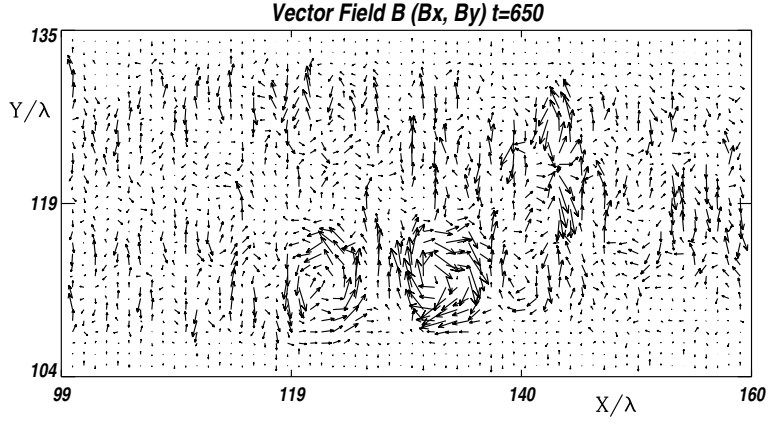

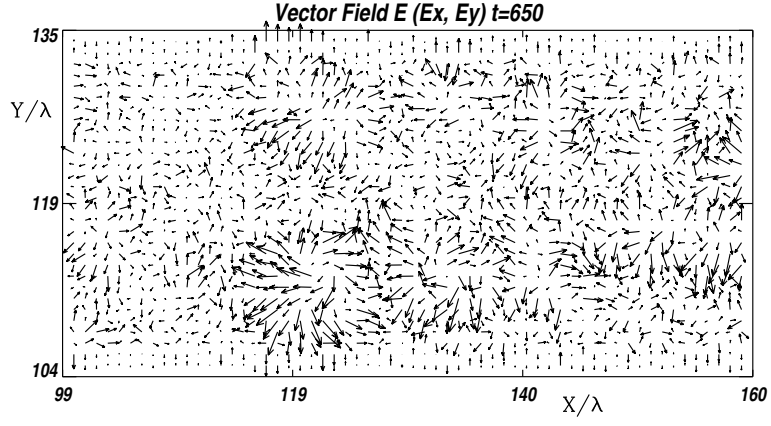

Hybrid structures

Structures from the pattern in the low-density region reveal a “hybrid” vortex-soliton nature with both oscillating and quasi-static components

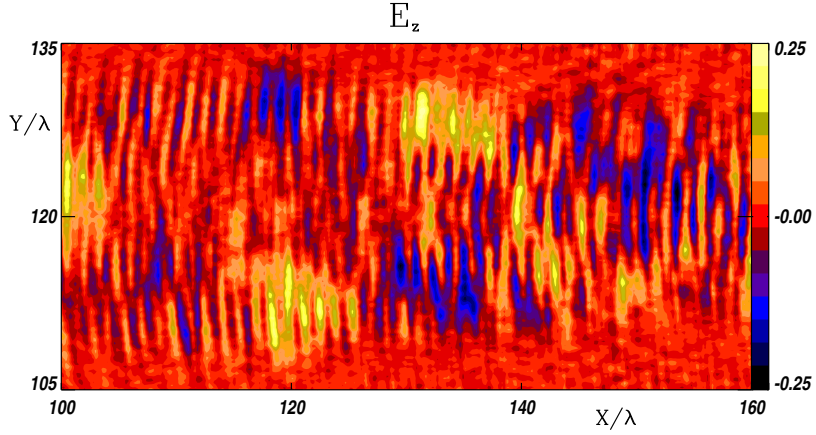

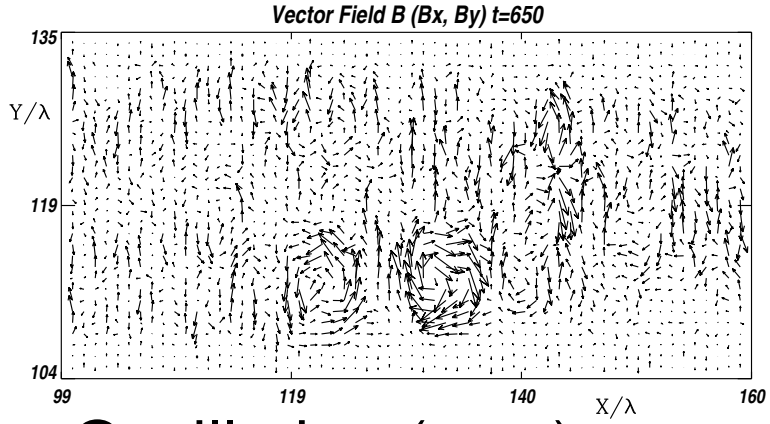

Oscillating (0.1ω)

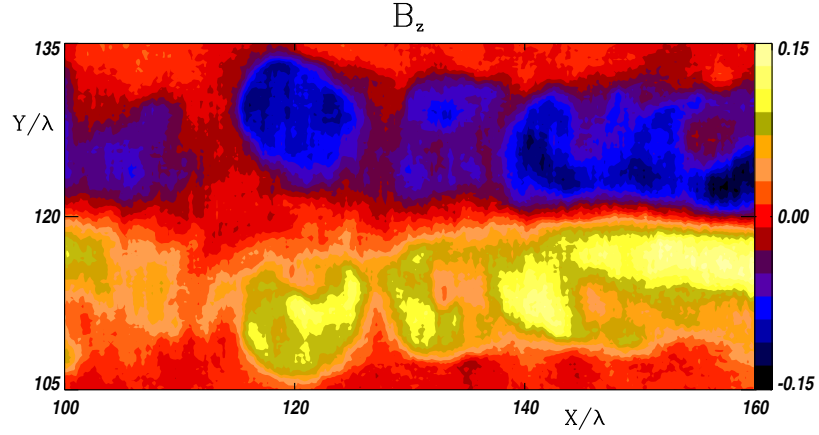

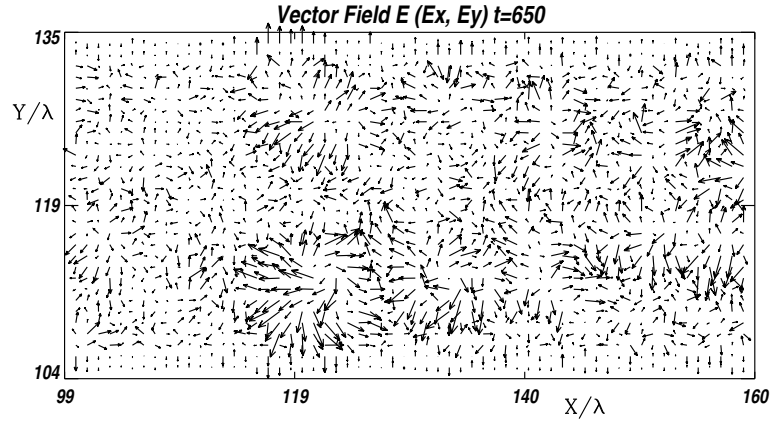

Quasi-static

Hybrid structures

Structures from the pattern in the low-density region reveal a “hybrid” vortex-soliton nature with both oscillating and quasi-static components

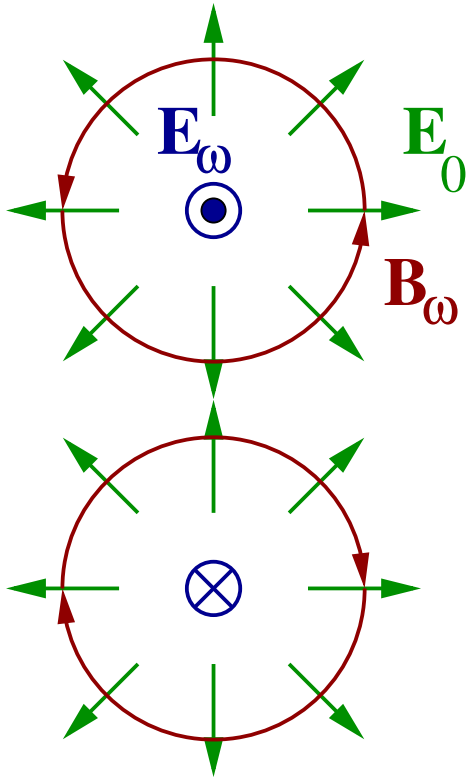

Antisymmetric “soliton” fields: oscillating E_z, B_x and B_y and electrostatic E_x, E_y

Hybrid structures

Structures from the pattern in the low-density region reveal a “hybrid” vortex-soliton nature with both oscillating and quasi-static components

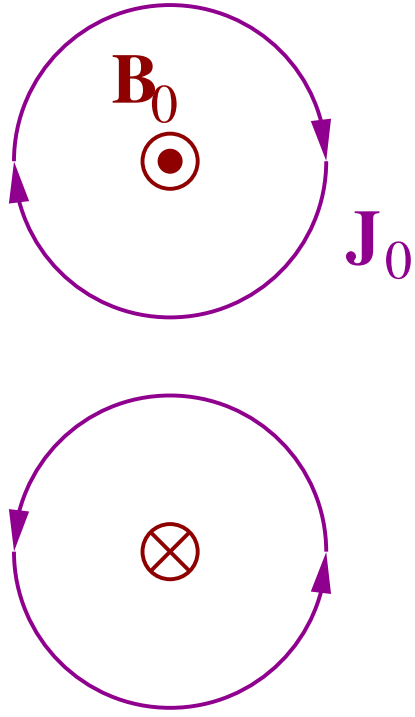

Antisymmetric “vortex” fields: static B_z, J_x and J_y

Hybrid structures

Structures from the pattern in the low-density region reveal a “hybrid” vortex-soliton nature with both oscillating and quasi-static components

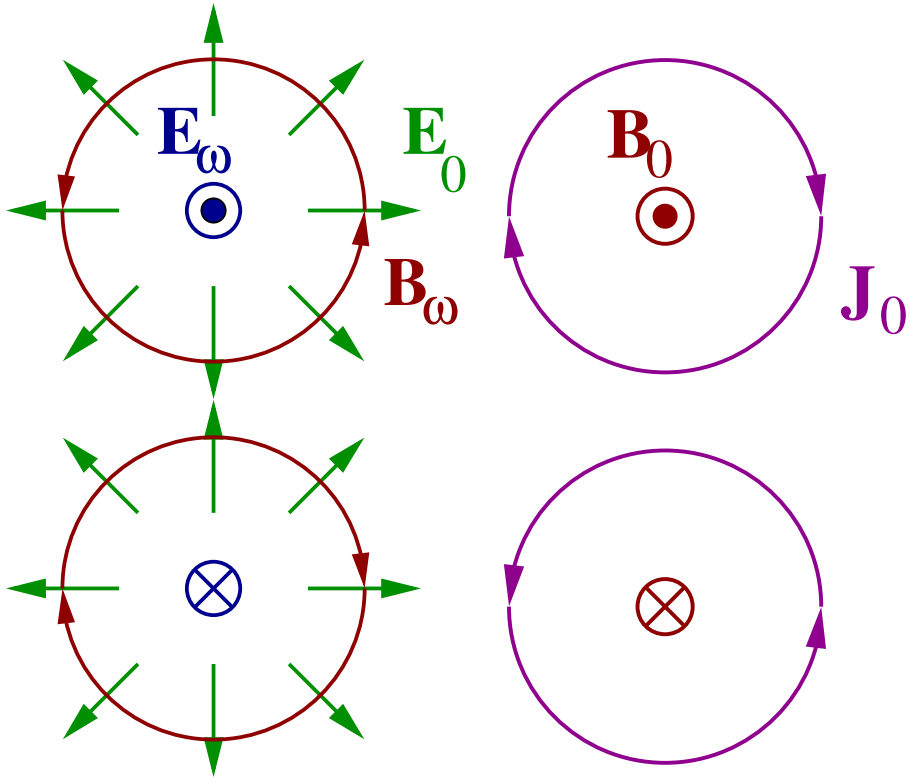

Toroidal structures in 3D?

Conclusions

Conclusions

- Effects of the ion dynamics following self-channeling have been unfolded

Conclusions

- Effects of the ion dynamics following self-channeling have been unfolded
- Various types of coherent structures have been observed in simulations

Conclusions

- Effects of the ion dynamics following self-channeling have been unfolded
- Various types of coherent structures have been observed in simulations
- Next steps:

Conclusions

- Effects of the ion dynamics following self-channeling have been unfolded
- Various types of coherent structures have been observed in simulations
- Next steps:
  - hybrid structures in 3D

Conclusions

- Effects of the ion dynamics following self-channeling have been unfolded
- Various types of coherent structures have been observed in simulations
- Next steps:
  - hybrid structures in 3D
  - experimental comparison